# 报送博士学位论文简况表

| 论文题目 | 槽式太阳能热发电系统的性能分析 | | |
|---|---|---|---|
| 作者姓名 | TRAORE MODIBO KANE | 授予学位的学科、专业 | 热能工程 |
| 作者单位 | 马里 | 地　址 | 巴马科 |
| 导师姓名 | 马重芳 | 专　业<br>技术职务 | 热能工程 |
| 导师单位 | 北京工业大学 | 地　址 | 北京市　朝阳区 平乐园100号 |
| 论文隶属学科分类号[注1]：TK124 | | | |
| 论文关键词[注2]：抛物槽，集热管;热损失;性能分析 | | | |


## 摘　要

抛物槽集热系统，在高达数百兆瓦范围内的太阳能领域,开发成在 200-350℃温度范围内应用的太阳能发电应用程序。搜集系统的新支撑结构设计，包括概念的研究，风洞测量，导致一个中心框架原件。这一新的转矩框设计比较其他的设计，能使搜集系统重量降低和较少变形。

因此，所有搜集系统连接着一个驱动器，这样减少了连接驱动器的管道数量，从而降低安装成本和热量消耗。目前的设计具有较高的系统效率（提高太阳能集热器效率，制定未来发展的最佳工厂的经营战略，推荐将来发展区域），本项目最重要的目标。 进行热量损耗测试和光学效率测试，创建一个集热器/接收器效率曲线图，以评估接收器内流体液体热量传导过程中的热量。为解决能量均衡问题，接收器管道的温度设置为 350K 和周围的温度假定为 300K。对于不同的流动条件，各种再循环和温度场围绕的接收管被吸收。当风速低时（基于采集器上的口径 $Re \leq 4.5\times10^5$），平均数量的接收管方位，对于集热器的影响是微不足道的。但是，当风速高时，吸收管道的玻璃罩周围变化对于集热器的影响是相当大的。


| 论文在何时何地以何种方式发表 | | | | | |
|---|---|---|---|---|---|
| 获得学位日期 | | 报送日期 | | 备　注 | |
| 收藏单位：北京图书馆（中国国家图书馆）。执行部门：国内资料组。 | | | | | |

注 1. 一般应注明《中国图书资料分类法》的类号

2. 为了文献标引工作从论文中选取出来用以表示全文主题内容信息款目的单词或术语。每篇论文选取 3~8 个词作为关键词。为了国际交流，应标注与中文对应的英文关键词。

# 报送博士学位论文简况表（英文）

| | | | |
|---|---|---|---|
| 论文题目 | PERFORMANCE ANALYSIS OF SOLAR PARABOLIC TROUGH SYSTEMS FOR ELECTRIC POWER GENERATION | | |
| 作者姓名 | TRAORE MODIBO KANE | 授予学位的学科、专业 | THERMAL ENGINEERING |
| 作者单位 | BEIJING UNIVERSITY OF TECHNOLOGY | 地　址 | 100 Ping le Yuan Chaoyang District |
| 导师姓名 | MA CHONG FANG | 专　业<br>技术职务 | THERMAL ENGINEERING |
| 导师单位 | BEJING UNIVERSITY OF TECHNOLOGY | 地　址 | 100 Ping le Yuan Chaoyang District |
| 论文隶属学科分类号[注1]: TK124 | | | |
| 论文关键词[注2]: Parabolic trough; Receiver tube; Heat loss; Performance analysis | | | |


ABSTRACT

A parabolic collector through system was developed for solar electricity generating application in the 200-350℃ temperature range in solar fields up to hundreds megawatts range. The design of new support structure of the collector includes concept studies, wind tunnel measurements and result in a structure with a central framework element. This new torque box design will have lower weight and less deformation design of the collector structure then the other designs considered.

Therefore, all the collector elements are connected on one drive, which result in reduced total number of drives interconnecting pipes, thus reducing the installation cost and thermal losses. The present design has a high system efficiencies (Improving the efficiency of solar energy collector, Developing an optimum plant operating strategy, Suggest area for future developments) the most important goals of this project.

The heat-loss testing and optical efficiency testing were carried out to create a collector/receiver efficiency curve that estimates the heat gain to the heat transfer fluid flowing within the receiver. For solution of the energy equation, temperature of the receiver tube is taken as 350K and ambient temperature is assumed to be 300K. Various recirculation and temperature fields were absorbed around the receiver tube for different flow conditions. Effect of collector orientation on the average Nu number for the receiver tube was found negligible when the winds speed is low ($Re \leq 4.5 \times 10^5$ based on the collector aperture). But when the wind velocity is high, the collector effect on the variation of Nu around the glass cover of the absorber tube is considerable.(可另附页)


| | | | | | |
|---|---|---|---|---|---|
| 论文在何时何地以何种方式发表 | | | | | |
| 获得学位日期 | | 报送日期 | | 备　注 | |
| 收藏单位：北京图书馆（中国国家图书馆）。执行部门：国内资料组。 | | | | | |

注 1. 一般应注明《中国图书资料分类法》的类号

2. 为了文献标引工作从论文中选取出来用以表示全文主题内容信息款目的单词或术语。每篇论文选取 3~8 个词作为关键词。为了国际交流，应标注与中文对应的英文关键词。。

# 独 创 性 声 明

本人声明所呈交的论文是我个人在导师指导下进行的研究工作及取得的研究成果。尽我所知，除了文中特别加以标注和致谢的地方外，论文中不包含其他人已经发表或撰写过的研究成果，也不包含为获得北京工业大学或其它教育机构的学位或证书而使用过的材料。与我一同工作的同志对本研究所做的任何贡献均已在论文中作了明确的说明并表示了谢意。

签名：_____ 日期：09/06/28

# 关于论文使用授权的说明

本人完全了解北京工业大学有关保留、使用学位论文的规定，即：学校有权保留送交论文的复印件，允许论文被查阅和借阅；学校可以公布论文的全部或部分内容，可以采用影印、缩印或其他复制手段保存论文。

（保密的论文在解密后应遵守此规定）

签名：_____ 导师签名：_____ 日期：09/06/28

# Abstract

A parabolic collector through system was developed for solar electricity generating application in the 200-350℃ temperature range in solar fields up to hundreds megawatts range. The design of new support structure of the collector includes concept studies, wind tunnel measurements and result in a structure with a central framework element. This new torque box design will have lower weight and less deformation design of the collector structure then the other designs considered.

Therefore, all the collector elements are connected on one drive, which result in reduced total number of drives interconnecting pipes, thus reducing the installation cost and thermal losses. The present design has a high system efficiencies (Improving the efficiency of solar energy collector, Developing an optimum plant operating strategy, Suggest area for future developments) the most important goals of this project.

The heat-loss testing and optical efficiency testing were carried out to create a collector/receiver efficiency curve that estimates the heat gain to the heat transfer fluid flowing within the receiver. For solution of the energy equation, temperature of the receiver tube is taken as 350K and ambient temperature is assumed to be 300K. Various recirculation and temperature fields were absorbed around the receiver tube for different

flow conditions. Effect of collector orientation on the average Nu number for the receiver tube was found negligible when the winds speed is low ($Re \leq 4.5 \times 10^5$ based on the collector aperture). But when the wind velocity is high, the collector effect on the variation of Nu around the glass cover of the absorber tube is considerable.

Key words: Parabolic trough; Receiver tube; Heat loss; Performance analysis

# Table of contents

# Chapter 1 Introduction

High efficiency Solar Thermal Electricity Generating Systems would be one of the more effective alternatives to meet the coming energy crisis and global environmental problems in the world. Among them, Solar Parabolic Trough Systems are becoming the most proven because of two advantages:

- Electricity generating: Some works have been done on this area. But the uses of combined system, of SPTS with Single Screw expender Technologies, would increase the effectiveness of those systems.
- Heat supply (Industrial Process Heat, Heating)

A distinct advantage of Solar Thermal Electricity Generating Systems with other renewable energies, such as photovoltaic (PV) and wind, is the possibility of using relatively cheap storage systems. That is, storing the thermal energy itself. Storing electricity is much more expensive.

In addition to above mentioned advantages its modular character, hybrid working (utilization of fuel, biogas or natural gas in absence of solar radiation) improve the quality of produced electricity and increases the capacity factor of this system, while reducing the cost price of produced kWh.

# Chapter 2 System description

## 2.1 Description of existing systems

Solar Parabolic though technologies are currently the most proven solar thermal electric technologies in the world. This is primarily due to nine large commercial scale solar power plants installed in USA. Large fields of parabolic trough collectors, as shown in figure 3-4, supply the thermal energy needed to produce steam for a Rankin steam turbine/generator cycle. Parabolic collectors have been used or are under construction for commercial power plants in many countries such as Mexico, Spain, Egypt, and Greece.

Figure 1 shows a process flow diagram that is a representative of the majority of parabolic trough solar power plants in operation today. The collector field consists of a large field of single-axis tracking parabolic collectors. The solar field is modular in nature and is composed of many parallel rows of solar collectors aligned on a north-south horizontal axis. Each solar collector has a linear parabolic-shaped reflector that focuses the sun's direct bean radiation on a linear receiver located at the focus line of the parabola. The collectors track the sun from east to west during the day to ensure that the sun is continuously focused on the linear receiver. A heat transfer fluid (HTF) is heated as it circulates through the receiver

and returns to a series of heat exchangers in the power block where the fluid is used to generate high-pressure superheated steam. The superheated steam is then fed to a conventional steam turbine/generator to produce electricity. The spent steam from the turbine is condensed in a standard condenser and returned to the heat exchangers via condensate and feed water pumps to be transformed back into steam. Condenser cooling is provided by mechanical draft wet cooling towers. After passing through the HTF side of the solar heat exchangers, the cooled HTF is re-circulated through the solar field.

### 2.1.1 History

Historically, parabolic trough plants have been designed to use solar energy as the primary energy source to produce electricity. The plants can operate at full rated power using solar energy alone, giving sufficient solar input. During summer months, the plants typically operate for 10 to 12 hours a day at full-rated electric output. However, today, all plants have been hybrid solar/fossil plants; this means they have a backup fossil-fired capability that can be used to supplement the solar output during periods of low solar radiation. In the system shown in Figure 1, the optional natural-gas-fired HTF heater situated in parallel with the solar field, or the optional gas steam boiler/reheater located in parallel with the solar heat exchangers, provide this capability. The fossil backup

can be used to produce rated electric output during overcast or nighttime periods. Figure 1 also shows that thermal storage is a potential option that can be added to provide dispatch ability.

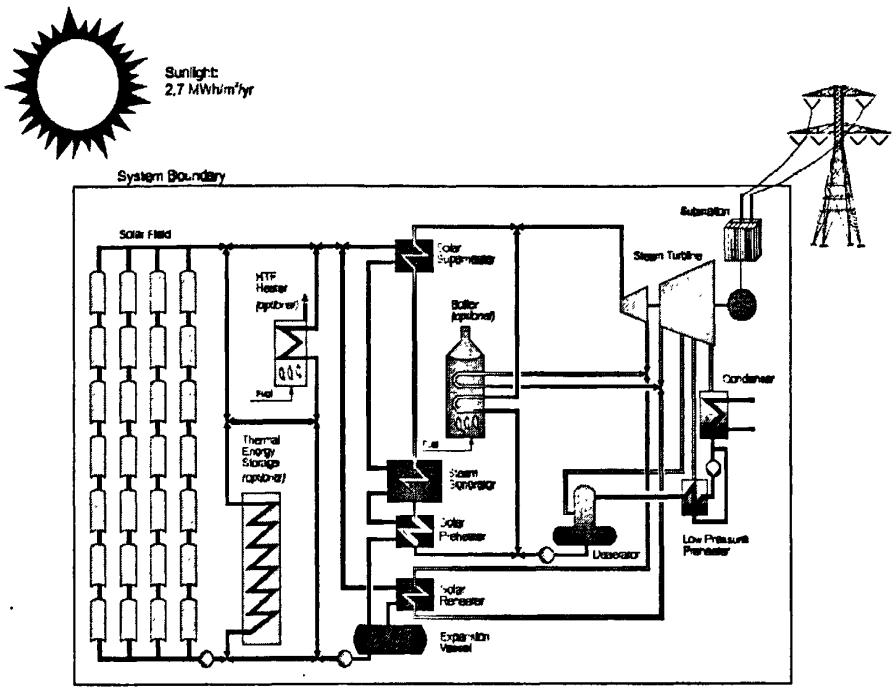


Fig.1 Solar/Rankine parabolic trough system schematic [23]

## 2.1.2 Integrated Solar Combined Cycle System

Integrated Solar Combined Cycle System (ISCCS) is also a new design concept to improve trough solar systems efficiency. The ISCCS is a new design concept that integrates a parabolic trough plant with a gas turbine combined-cycle plant. The ISCCS has generated much interest because it offers an innovative way to reduce cost and improve the overall solar-to-electric efficiency. A process flow diagram for an ISCCS is shown in Figure 2. The ISCCS uses solar heat to supplement the waste

heat from the gas turbine in order to augment power generation in the steam Rankine bottoming cycle. In this design, solar energy is generally used to generate additional steam and the gas turbine waste heat is used for preheat and steam superheating. Most designs have looked at increasing the steam turbine size by as much as 100%. The ISCCS design will likely be preferred over the solar Rankine plant in regions where combined cycle plants are already being built.

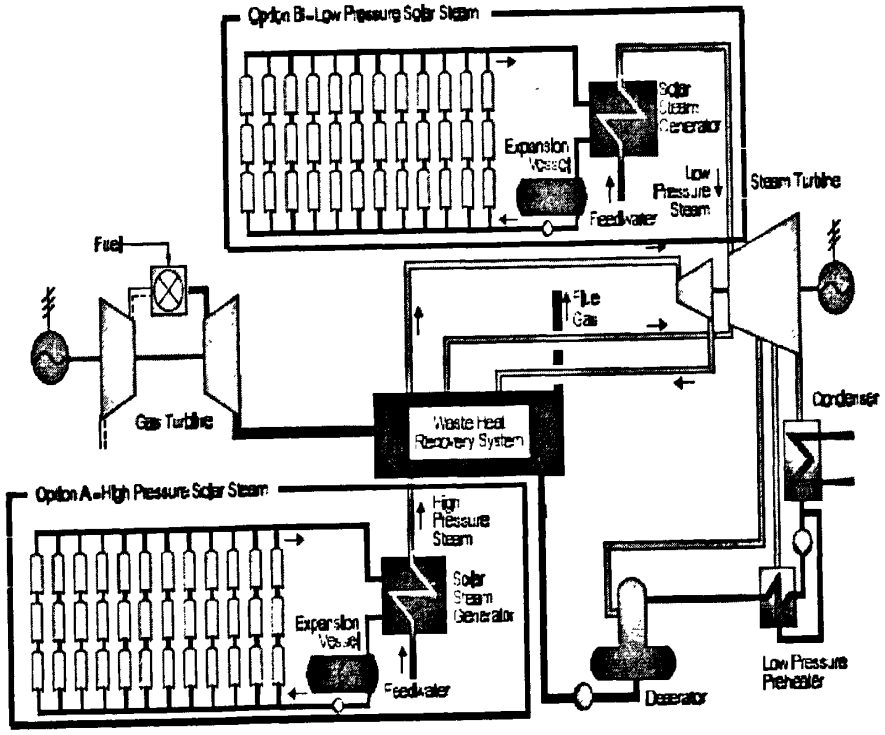


Fig.2 Integrated Solar Combined Cycle System [23]

### 2.1.3 Advances in parabolic trough solar system in the world

Organized, large-scale development of solar collectors began in U.S.A. in the mid-1970s under the Energy Research and Development Administration (ERDA) and continued with the establishment of the U.S. Department of Energy (DOE) in 1978. Parabolic trough collectors capable of generating temperatures greater than 500°C (932°F) were initially developed for industrial process heat (IPH) applications. Much of the early development was conducted or sponsored by Sandia National Laboratories in Albuquerque, New Mexico. Numerous process heat applications, ranging in size from a few hundred to about 5000 $m^2$ of collector area, were put into service. Acurex, SunTec and Solar Kinetics were the key parabolic trough manufacturers in the United States during this period.

Parabolic trough development also took place in Europe and culminated with the construction of the IEA Small Solar Power Systems Project/Distributed Collector System (SSPS/DCS) in Tabernas, Spain, in 1981. This facility consisted of two parabolic trough solar fields with a total mirror aperture area of 7602 $m^2$. The fields used the single-axis Acurex collectors and the double-axis tracking parabolic trough collectors developed by M.A.N. of Munich,

Germany. In 1982, Luz International Limited (Luz) developed a parabolic trough collector for electricity generation that was based largely on the experience that had been gained by DOE/Sandia and the SSPS projects.

Although several parabolic trough developers sold IPH systems in the 1970s and 1980's, they generally found two barriers to successful marketing of their technologies. First, there was a relatively high marketing and engineering effort required for even small projects. Second, most potential industrial customers had cumbersome decision-making processes which often resulted in a negative decision after considerable effort had already been expended.

In 1983 Southern California Edison (SCE) signed an agreement with Acurex Corporation to purchase power from a solar electric parabolic trough power plant. Acurex was unable to raise financing for the project. Consequently, Luz negotiated similar power purchase agreements with SCE for the Solar Electric Generating System (SEGS) I and II plants. Later, with the advent of the California Standard Offer (SO) power purchase contracts for qualifying facilities under the Public Utility Regulatory Policies Act (PURPA), Luz was able to sign a number of SO contracts with SCE that led to the development of the SEGS III through SEGS IX projects. Initially, the plants were limited by PURPA to 30 MW

in size; later this limit was raised to 80 MW. Table 1 shows the characteristics of the nine SEGS plants built by Luz.

In 1991 Luz fell to bankruptcy when it was unable to secure construction financing for its tenth plant (SEGS X). Though many factors contributed to the demise of Luz, the basic problem was that the cost of the technology was too high to compete in the power market. Lotker[5] describes the events that enabled Luz to successfully compete in the power market between 1984 and 1990 and many of the institutional barriers that contributed to their eventual downfall.

Tab.1 Characteristics of SEGS I though IX [24]

| SEGS plant | Year of operation | Net output MW | output temp.℃ | Solar field area,$m^2$ | Solar turbine eff.% | Annual output MWh |
|---|---|---|---|---|---|---|
| I | 1985 | 13.8 | 307 | 82960 | 31.5 | 30.1 |
| II | 1986 | 30 | 316 | 190338 | 29.4 | 80.5 |
| III&IV | 1987 | 30 | 349 | 230300 | 30.6 | 92.78 |
| V | 1988 | 30 | 349 | 250500 | 30.6 | 91.82 |
| VI | 1989 | 30 | 390 | 188000 | 37.5 | 90.85 |
| VII | 1989 | 30 | 390 | 194280 | 37.5 | 92.646 |
| VIII | 1990 | 80 | 390 | 464340 | 37.6 | 252.75 |

| | | | | | | |
|---|---|---|---|---|---|---|
| IX | 1991 | 80 | 390 | 483960 | 37.6 | 256.125 |

It is important to note that all of the SEGS plants were sold to investor groups as independent power projects and continue to operate today. Table 1 shows the characteristics of SEGS I though IX solar collectors from 1985 to 1991.

**Figure 3 Array of trough collectors [6]**

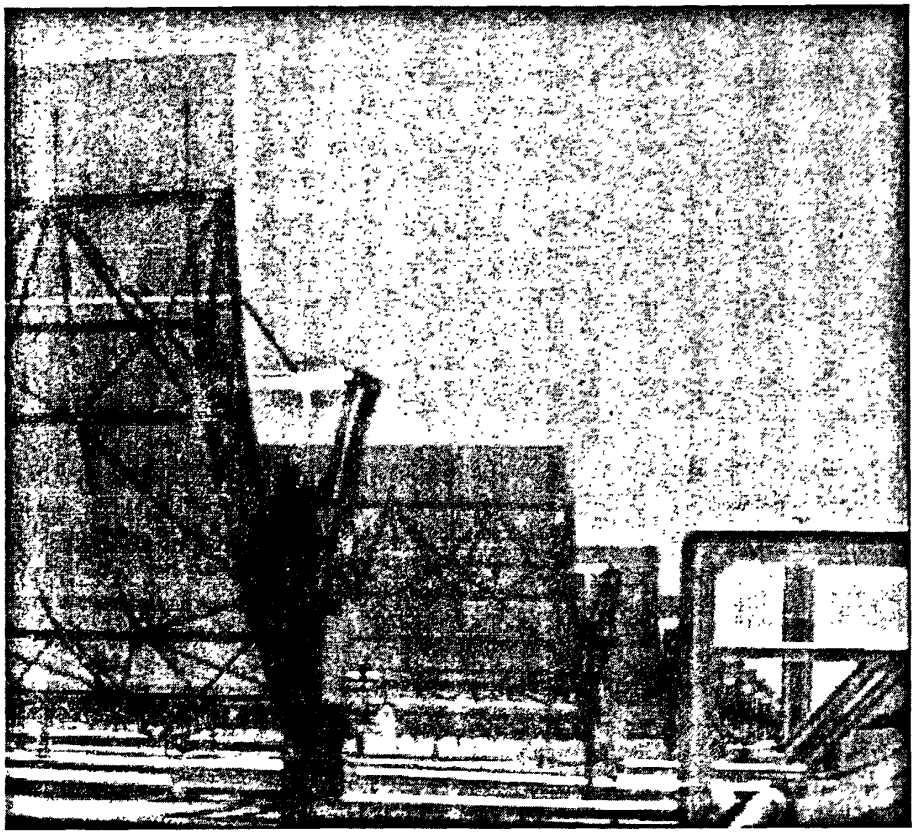

**Figure 4 Heat transfer fluid loop of a trough system** [6]

Luz System Three (LS-3) SCA: The LS-3 collector, as shown in figure 5, was the last collector design produced by Luz and was used primarily at the larger 80 MW plants. The LS-3 collector represents the current state-of-the-art in parabolic trough collector design and is the collector that would likely be used in the next parabolic trough plant built. A more detailed description of the LS-3 collector and its components follows.

The linear receiver also referred to as a heat collection element (HCE), is one of the primary reasons for the high efficiency of the Luz parabolic

trough collector design. The HCE consists of a 70 mm steel tube with a cermet selective surface, surrounded by an evacuated glass tube. The HCE incorporates glass-to-metal seals and metal bellows to achieve the vacuum-tight enclosure.

The vacuum enclosure serves primarily to protect the selective surface and to reduce heat losses at the high operating temperatures. The vacuum in the HCE is maintained at about 0.0001 mm Hg (0.013 Pa). The cermet coating is sputtered onto the steel tube to give it excellent selective heat transfer properties with an absorptance of 0.96 for direct beam solar radiation, and a design emissivity of 0.19 at 350°C (662°F). The outer glass cylinder has anti-reflective coating on both surfaces to reduce reflective losses of the glass tube. Getters, metallic substances that are designed to absorb gas molecules, are installed in the vacuum space to absorb hydrogen and other gases that permeate into the vacuum annulus over time.

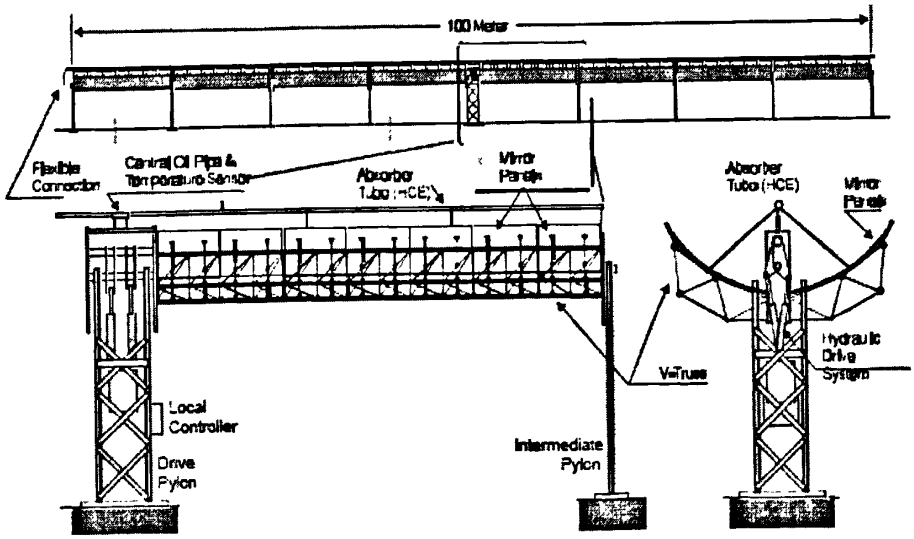

**Figure 5 Luz System Three Solar Collector Assemblies [23]**

The SCAs rotate around the horizontal north/south axis to track the sun as it moves through the sky during the day. The axis of rotation is located at the collector center of mass to minimize the required tracking power. The drive system uses hydraulic arms to position the collector. A closed loop tracking system relies on a sun sensor for the precise alignment required to focus the sun on the HCE during operation within +/- 0.1 degrees. The tracking is controlled by a local controller on each SCA. The local controller also monitors the HTF temperature and reports operational status, alarms, and diagnostics to the main solar field control computer in the control room. The SCA is designed for normal operation in winds up to 25 mph (40 km/h) and somewhat reduced accuracy in winds up to 35 mph (56 km/h). The SCAs are designed to withstand a maximum of 70 mph (113 km/h) winds in their stowed position (the collector aimed 30° below eastern horizon).

## 2.2 Description of the new system

The new system includes the receiver tubes, the concentrator, heat transfer fluid loop, and generator. See fig.6 and fig.7. The track system and collector structure support system are shown in figures 8-10.

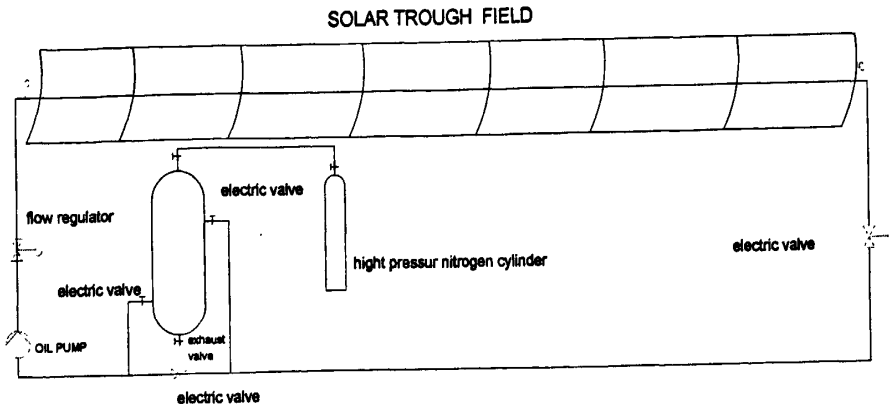


**Figure.6 Flow diagram Collector sub -system**

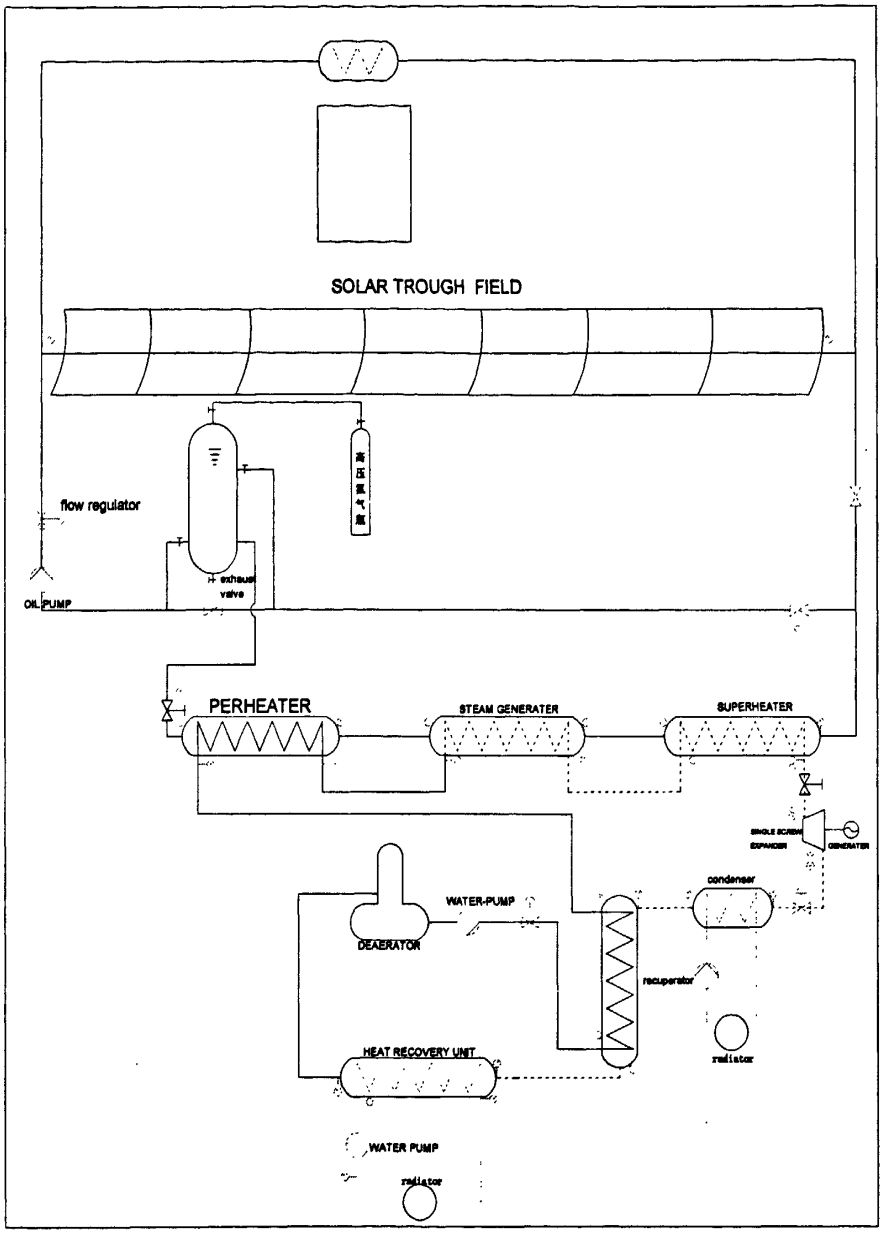


**Figure.7 Flow diagram of the whole system**

**Table 2: Characteristics of the new system**

| Layout | Parabolic trough collector |
|---|---|
| Support structure | Steel frame work, |
| Collector length | 12 m |
| Drive | Electric drive |
| Max. wind speed | 20m/s |
| parabola | $y = \frac{x^2}{4f}$ with f = 1.71 m |
| Aperture width | 5.77 m |
| Reflector | 4 aluminum facets |
| Receiver tube | Evacuated glass envelope |
| Fluid | oil |

# Chapter 3 New system description and mounting

## 3.1 Selecting the reflector geometry

Selecting optimum geometry of mirror facets (shape, size) excessive heat loss could be avoided. The collector model used in this study is a parabola having the equation,

$$y = \frac{x^2}{4f}.$$

The rays of light parallel to the axis of a mirrored parabola will mostly be reflected and focused at the focal point at a distance $f$ from the vertex. This effect can be used in a linear arrangement, where a mirrored ``trough`` with a parabolic cross section will focus solar radiation on a line focus, which is pointed directly at the sun.

## 3.2 Collector module size

The collector models are made up of three identical 12000mm long collector modules, as shown in Figure 8. Each module comprises 36 parabolic mirror panels and 9 along the horizontal axis between pylons and 4 in a vertical cross-section. Each mirror is supported on the structure

at four points on its backside. This permits the panel to bend within the range of its flexibility without effect on the focal point.

## 3.3 Steel structure design

Based on existing design a so-called torque-box design has bee selected for the present study with less weight and less deformations of the collector structure. This reduces torsion and bending of the structure during operation and results in increased optical performance and wind resistance.

See Figure 9 the central element of the box design is a 12-m long steel space-frame structure having a squared cross section that holds the support arms, as shown in Figures 10, 11 and 12 for the parabolic mirror facets. The torque box is built out of only 4 different steel parts. This leads to easy manufacturing.

The design utilizes mirror supports that make use of the aluminum facets as static structural elements, but at the same time reduce the forces on the aluminum sheets by a factor free. This promises less deformation with highest wind speeds. Absorber tube supports were designed such to reduce the breakage risk and to ease mirror cleaning in comparison to the existing. The majority of the structural parts are produced with steel construction tolerances.

The collector system is tracked with the sun during operation along

their long axis with an electric drive. The drive system consists of electrical system mounted on the central drive pylon.

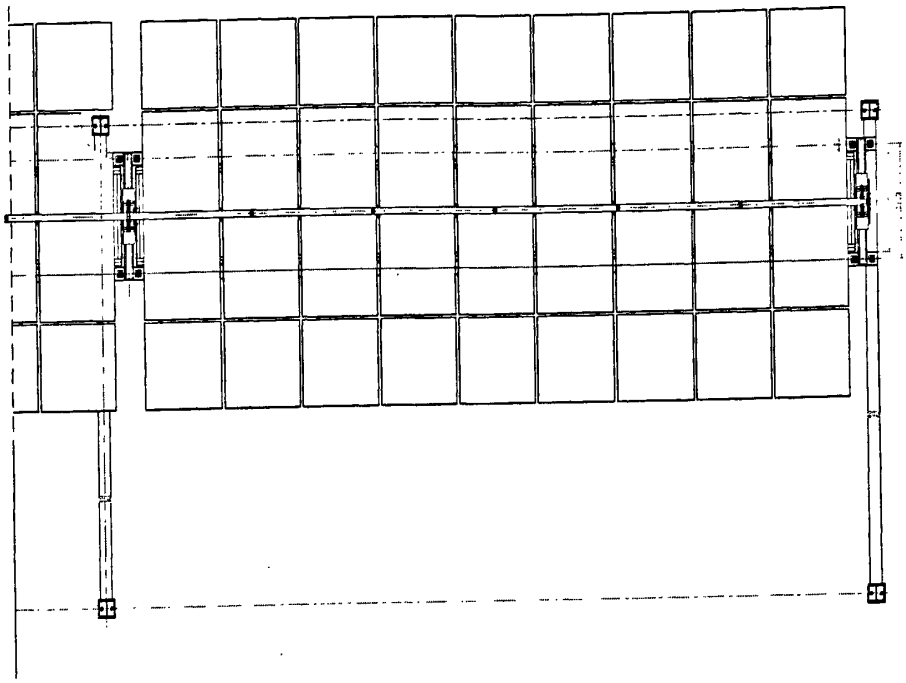

**Figure.8 Reflector module mounting**

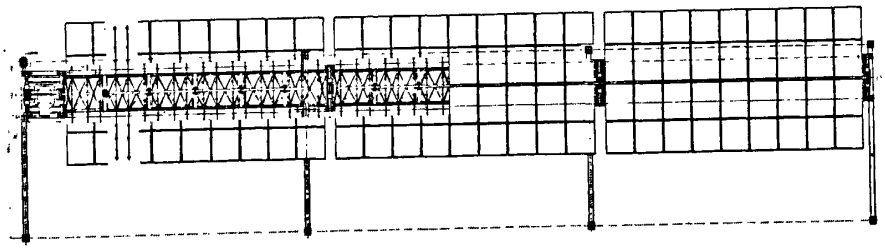

**Figure.9 Torque box structure**

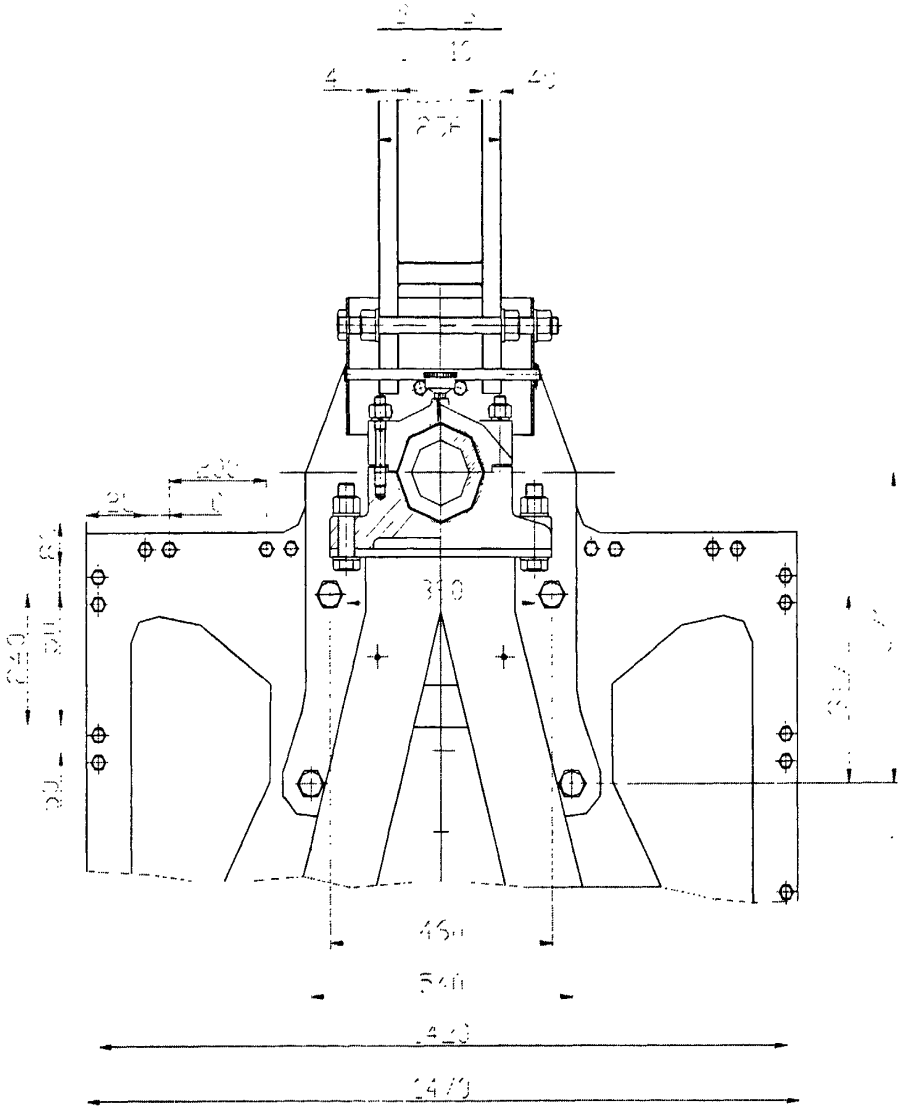

**Figure.10 Arm assembly system**

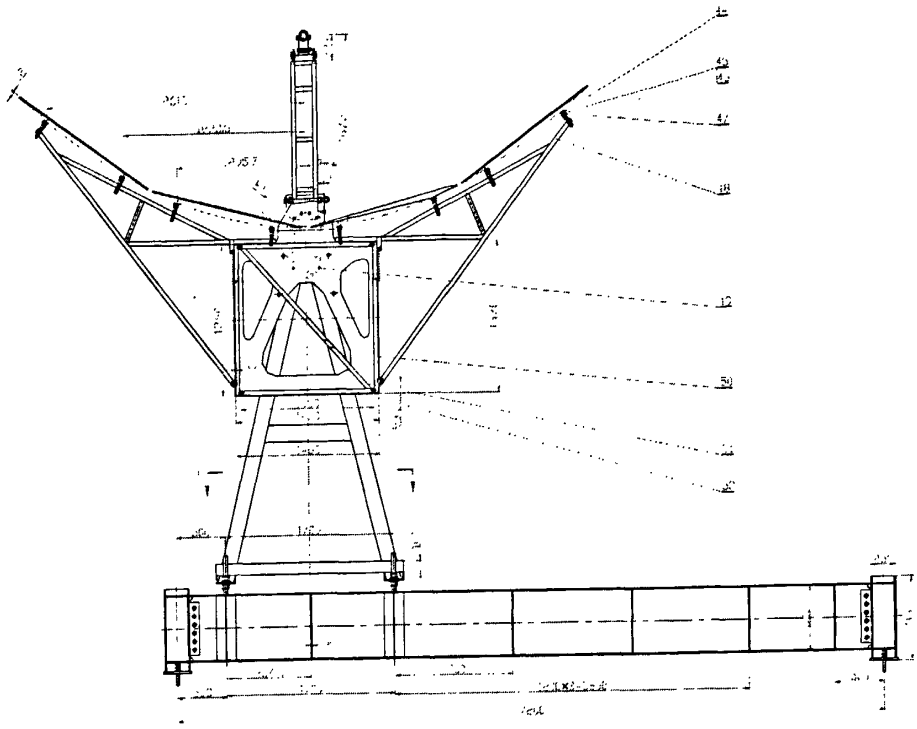

**Figure.11 Structure support assembly**

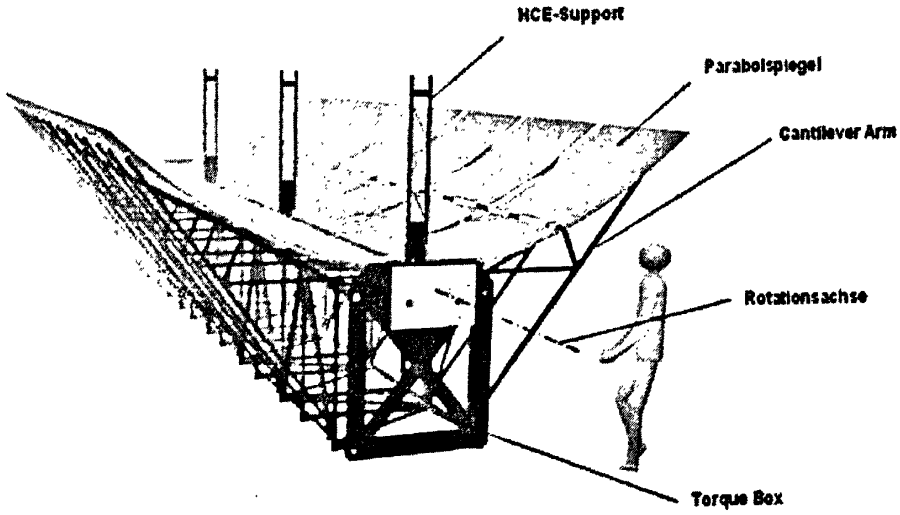


**Figure 12 Effect Picture of trough collector [18]**

# Chapter 4 Receiver Heat Loss Test

## 4.1 Test-Stand description

The operation of any solar thermal energy collector can be described as an energy balance between the solar energy absorbed by the collector and the thermal energy removed or lost from the collector. The system efficiency could depend on several parameters. Fig. 14 and Fig. 15 are the photographs of the Key Laboratory of Enhanced Heat Transfer and Energy Conservation Heat Loss Test Stand. This test stand is located in the lab number 506 and uses electric resistance heating on the inside of the HCE to bring the absorber surface up to desired test temperatures. Once a desired temperature is reached and the system comes to steady state, power transducers measure the electric power required to maintain the absorber temperature. The power required is the heat loss from the HCE to the environmental.

**Figure.13 Heat loss test stand assemblies in the lab**

**Figure.14 Heat loss test stand assemblies in the lab**

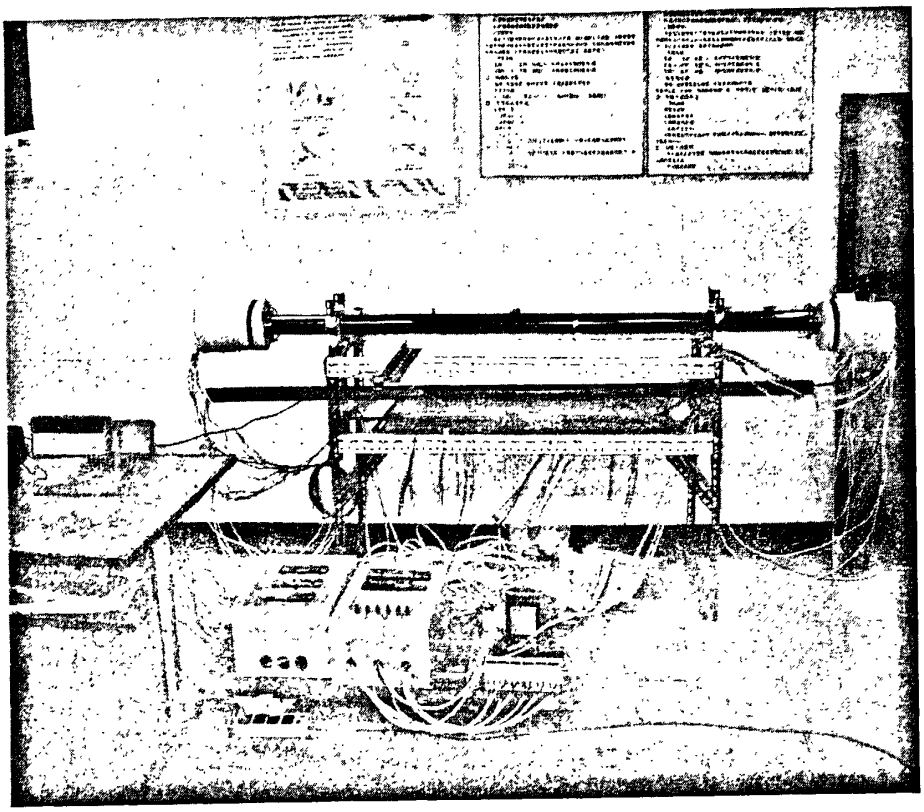

**Figure 15 Heat loss stand in lab**

Present HCEs is 2m long with an absorber inner diameter of 59.5mm. To test HCE heat loss, two copper pipes 114cm long each and outer diameter 4.9cm are inserted into the ends of an HCE-one copper pipe per end. Bolt heads protruding from the copper pipe surface center it in the HCE and prevent it from touching the inner absorber surface. The copper pipe evens out the temperature distribution generated by four internal electric resistance heaters. Two of the heaters are 4-cm-long, stainless-steel-sheathed, coiled cable heaters whose surfaces contact the interior of the copper pipe. The third heater, shown in Fig.17 is a 950mm inconel cartridge heater suspended along the cylindrical axis of the

copper pipe using inconel spacers. The cartridge heater is fully inserted into the copper pipe so that its innermost end is flush with the innermost end of the copper pipe. The coil heaters are held in position on the cartridge heater by shrink-fitted inconel spacers. When the copper pipe is inserted into the HCE, one coil heater ends up just inside the HCE, whereas the other is adjacent to it but just outside the HCE. The innermost coil heater compensates for end-loss effects, whereas the outermost coil heater is used to create an adiabatic boundary along the copper pipe between the two coil heaters and the two cartridge heaters. The cartridge heater, shown in Fig 16, supplies most of the thermal input to the system, especially at increasing absorber temperatures. Power transducers measure heater output. The total heat-loss is based on the sum of the powers of the two innermost coil heaters and the two cartridge heaters. Figure 18 shows one of the two heater assemblies, and table 3 lists heater and power transducer specifications.

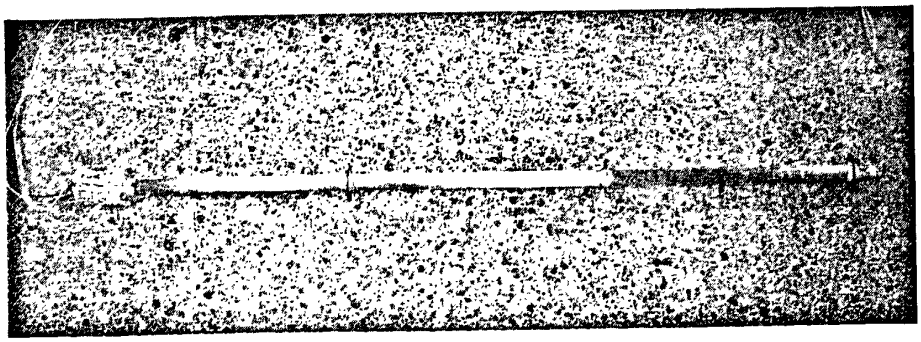

**Figure.16 Cartridge heater**

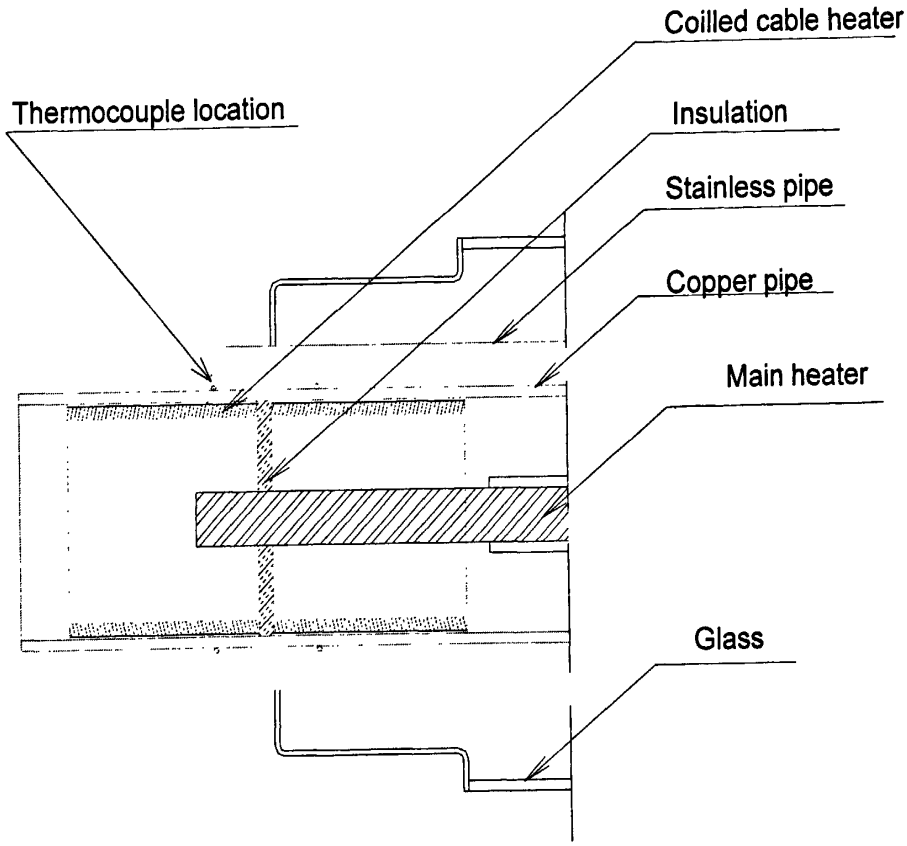


**Figure.17 Heater assembly**

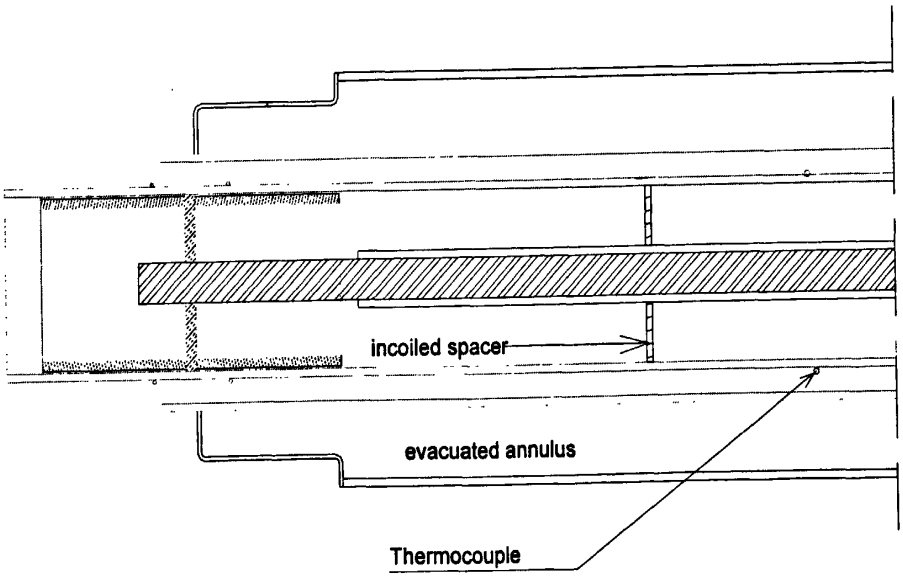


**Figure 18 Heaters and transducer assembly**

**Table 3 Heater and Power Transducer Specifications**

| Heater Type | Numb | Max. Power of each Heater(W) | Transducer Full-Scale Limit(W) | Error % of Full Scale | Error (W) |
|---|---|---|---|---|---|
| Coiled cable heater | 4 | 250 | 500 | 0.2% | 0.5 |
| Cartridge heater | 2 | 750 | 1500 | 0.2% | 1.5 |

Thermocouples measure the temperature of the copper pipe, stainless-steel absorber, and glass at the locations shown in Fig 17 and Fig 18. The copper end temperature is measured at two locations (two transducers by location), the absorber inner surface at one location, the heater surface at one location (two transducers by location) and the glass at one location. The heating assembly and thermocouple locations for the other half are identical and symmetrical about the HCE center line. The ends of copper pipes touch when both heating assemblies are inserted into an HCE. Inconel, copper, and stainless steel have different linear expansion coefficients. Cares have been taken to attach the copper and inconel at only one point to avoid thermal stresses. The center of the HCE

is the approximate location of this attachment.

Wires attach the thermocouples to the copper and glass surfaces. The thermocouples measuring absorber temperature spring out from the copper pipe to contact the inner absorber surface. Reliable absorber temperature measurement requires good contact between the thermocouple and the absorber, as well as local radiation shielding to prevent radiant heating of the thermocouple by the copper pipe. Figure 19 shows the shielding underneath one thermocouple used to measure absorber temperature, and Table 4 lists the thermocouple specifications. Thermocouple measure also air and heater temperatures.

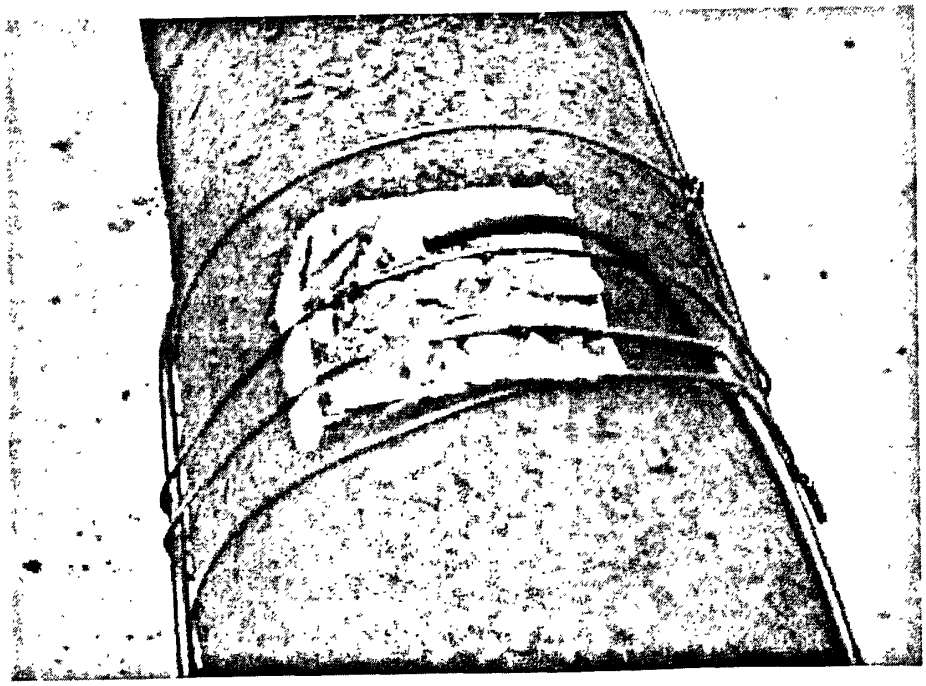

**Figure.19 Absorber thermocouple with required radiant shielding on copper pipe [22]**

Table.4 Thermocouple specifications

| Thermocouple Description | Calibration Type | Range ℃ | Temperature Error Maximum of % of reading | Temperature Error Maximum of ℃ |
|---|---|---|---|---|
| Alloy 600 sheath | K-special limits | 0-1200 | 0.5% | 6 |

## 4.2 Experience procedure

Testing proceeds once the heating assemblies are in place and the HCE is supported in the test stand. Electrical power to the inner coil and cartridge heaters is increased slowly until all absorber temperatures approach a value of interest (e.g., 400°C). The power to the outer coil heaters is adjusted so that the outer copper temperatures are equal to the inner copper temperatures, creating adiabatic boundaries between thermocouples shown in fig.17 -18. Temperatures and power values are logged every 5 seconds. Steady state is achieved when heater set-points are not changed and the center-of-glass and absorber temperatures remain constant (variation $\leq 0.5$°C) over a period of at least 15 minutes.

Once a desired temperature is reached and the system comes to steady state, power transducers measure the electric power required to maintain the absorber temperature. The power required is the heat loss from the

HCE to the environmental. Table 4 shows some experimental data.

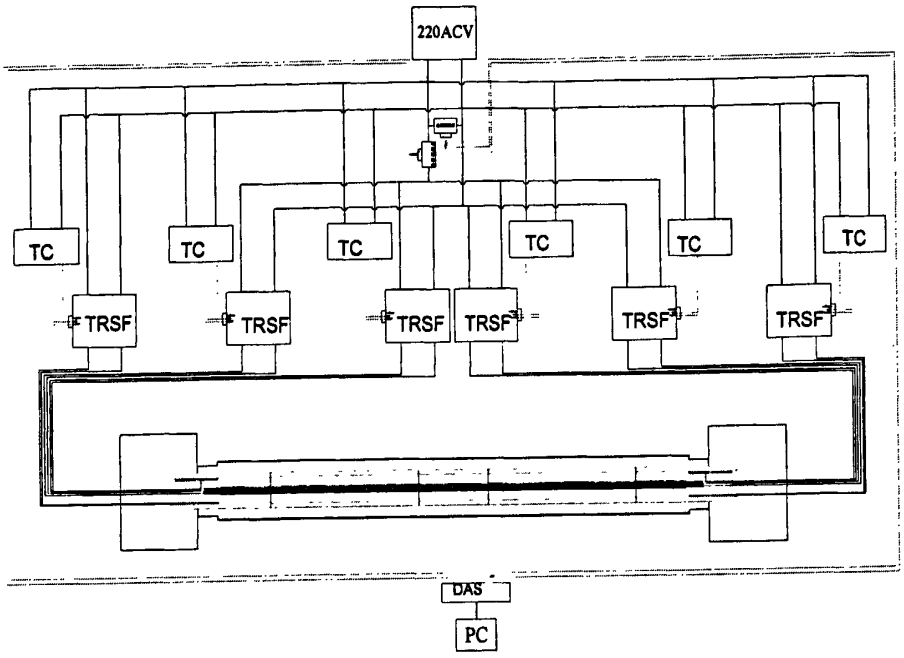


**Figure.19 Detailed installation schema**

## 4.3 Results and discussion

The heat –loss data for the given trough receiver is sown in Table 5.

**Table 5 Experimental data**

| TEST | Temp difference $\Delta T_{ave}$ | Heat loss W/m | Glass Temperature |
|---|---|---|---|
| 1 | 176.5 | 44.0 | 26.1 |
| 2 | 220.9 | 64.6 | 30.0 |
| 3 | 266.3 | 102.0 | 34.5 |

Data logged in Table.5 shown that the heat losses are within uncertainty.

# Chapter 5 Simulation of receiver heat loss

There are two different ways to evaluate the heat loss of HCE: on-work method and off-work method. The first method is used when the HCE is working (the system is running), and can only be used in daytime and collector field. It is very complicated to conduct the experiment by this way. The second way needs the direct and indirect sunlight to be prevented from the receiver tube in daytime, or can be conducted at sunny night or in the lab. The latter has been used to evaluate the heat loss of HCE based on the steady state equilibrium theory in literatures 1-2 and some conclusions have been made. The latter method has also been used to evaluate the heat loss of HCE based on the quasi-steady state theory in literatures 3-4 and some conclusions have been made. Because of the inconvenience of the latter method literatures[5-7] used the infrared camera and pyrometer to measure the outer surface temperature of glass envelop and absorber respectively and evaluate the heat loss of HCE qualitatively.

The existing experiments and simulations have been conducted on external factors such as constant wind velocity and different temperature differences. Those documents referred to other relative documents which present modeling heat transfer process of HCE. But the following problems as : (1) influence of selective coatings on heat loss of HCE; (2)

influence of annular pressure on heat loss of HCE; and (3) influence of wind velocity on heat loss of HCE remain.

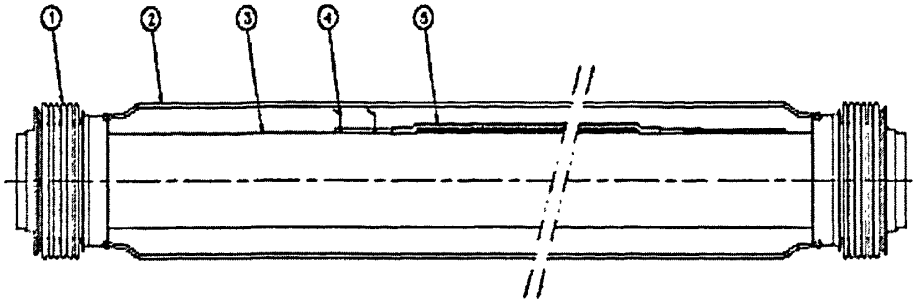


1. Bellow, 2. Glass envelops, 3. Absorber, 4. Getter, 5. Getter Bridge

**Figure.21 Model of parabolic trough receiver**

As the key part of the parabolic trough collector the design and optimization of HCE is very important. Off-work method and steady state equilibrium were used to study the influence of selective coatings, annular pressure, temperature difference $\Delta T$, wind velocity on the heat loss of HCE. Besides solving the above problems modeling of HCE as a basis of the following researches of parabolic trough collector is very important too.

## 5.1 Research on parabolic trough receivers

In a combination of radiactive, convective, and conductive energy transfers, the heat absorber tube loses power to the ambient, which was called as the heat loss of HCE.

For parabolic trough receivers the total collector thermal energy

output $\dot{q}_{col}$ is the absorbed thermal energy $\dot{q}_{abs}$, reduced by prevailing thermal losses $\dot{q}_{heatloss}$,

$$\dot{q}_{col} = \dot{q}_{abs} - \dot{q}_{heatloss} = \dot{q}_m (h_{out} - h_{in}) \qquad (1)$$

From equation(1) a conclusion can be made that the collector thermal energy output $\dot{q}_{col}$ is determined by operating conditions and is proportional to the change in enthalpy of the heat transfer fluid between the inlet and outlet of the receiver and mass flow rate $\dot{q}_m$.

### 5.1.1 Methods by Surface temperature measurements

It is not practical to measure the change in the enthalpy of the fluid between the inlet and outlet of receiver in a collector field. Because of this inconvenience the heat loss from receiver to ambient can be evaluated by measuring the outer surface temperature of the glass envelop with infrared camera or pyrometers with wave length in 7–14 μm range without regarding to the energy balance of absorber boundary. This method serves only as a relative measurement for the heat loss due to the strong dependence of glass temperature on coating properties, annulus vacuum level, irradiance, wind velocity, ground temperature, and sky temperature, but it can show some information on possible degradation of the selective coating and vacuum.

## 5.1.2 Methods of Quasi-steady-state equilibrium

If the absorber is placed in the position where direct and indirect irradiation are shielded then the absorbed energy by receiver $\dot{q}_{abs}$ is equal to zero and equation (1) can be simplified as equation (2) as follows:

$$\dot{q}_{heatloss} = q_m(h_{in} - h_{out}) = \dot{q}_{col} \qquad (2)$$

If the change in temperature between inlet and outlet of HCE is of a few centigrade , assuming a linear function of the heat losses with temperature, the average fluid temperature is used to calculate the temperature difference $\Delta T$[345]. Due to the small difference in temperature between fluid and wall adjacent to, the fluid temperature is considered to be identical to the absorber temperature.

## 5.1.3 Methods of Steady state equilibrium

Due to the complexity and higher cost to conduct the experiment via quasi-steady-state equilibrium steady state equilibrium can be used to simplify the test. Heaters are used to keep inner surface temperature of absorber uniformly and the receiver system in balance, and then power exhausted of heaters to keep receiver system in steady state equilibrium is equal to the heat loss at that temperature difference. Then the heat loss can be expressed in equation (3) as follows,

$$\dot{q}_{heatloss} = P_{heatsource} \qquad (3)$$

Results by this method will be more accurate than that by

quasi-steady-state equilibrium due its uniform temperature distribution in inner surface along the axis of the absorber.

## 5.2 Control equations of heat transfer process

Based on off-work method and steady state equilibrium aforementioned an empirical model was modeled to evaluate the thermal performance of heat loss of HCE. In order to simplify the modeling we assume that: end heat loss of HCE is negligible; in radial direction inside the absorber and the glass envelop temperature distribution of the wall is linear; heat conduction in circumferential directions of HCE is negligible; thermal resistance of absorber coating and glass envelope anti-reflection coating is negligible; thermal conductance of glass envelop wall is constant; absorber outer surface and glass envelop inner surface are gray and inside the annular space is diffuse irradiation and reflections; annular space is long, horizontal, concentric cylinders at uniform temperatures; annulus gas is nonparticipating; glass envelope is opaque to radiation in the infrared range; wind direction is normal to the axis of the HCE; Glass envelop is a Long isothermal horizontal cylinders; Effective sky temperature is 8℃ below the ambient temperature; HCE is small convex gray object in a large blackbody cavity.

Based on the above assumptions and off-work method with Steady state equilibrium the heat transfer of HCE can be simplified as a

two-dimensional heat transfer phenomena along its diameter[39], as shown in fig.22. Heat transfer is under steady state in each interface along the diameter.

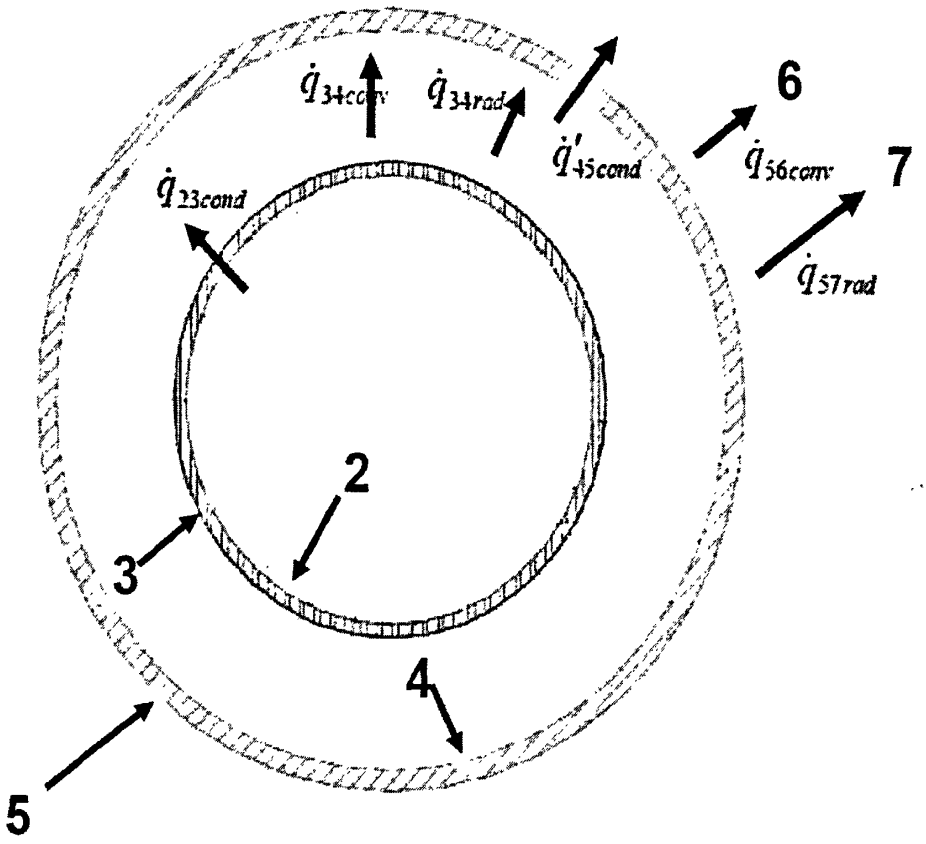


2—inner surface of steel absorber 3—outer surface of steel absorber 4—inner surface of glass envelop 5—outer surface of glass envelop 6—ambient air7—sky

**Fig.22 Steady state heat transfer process of two-dimensional parabolic trough receiver**

Based on fig.23 and energy conservation law we can write the following equations:

Energy balance on outer surface of steel absorber 3 is as follows,

$$\dot{q}_{23cond} = \dot{q}_{34conv} + \dot{q}_{34rad} \quad (4)$$

Energy balance on inner surface of glass envelop 4 is as follows,

$$\dot{q}_{34conv} + \dot{q}_{34rad} = \dot{q}_{45cond} \quad (5)$$

Energy balance on outer surface of glass envelop 5 is as follows,

$$\dot{q}_{45cond} = \dot{q}_{56conv} + \dot{q}_{57rad} \quad (6)$$

So, the heat loss from receiver to ambient can be expressed as follows,

$$\dot{q}_{HeatLoss} = \dot{q}_{56conv} + \dot{q}_{57rad} \quad (7)$$

## 5.3 Boundary conditions

Actually this model simulates the steady state equilibrium of heat transfer of HCE based on the off-work method, so the inner surface temperature of steel absorber $T_2$, temperature of ambient air $T_6$, sky temperature $T_7$ and wind velocity $V_6$ should be given as the boundary conditions. Other parameters such as annular pressure, emissivity of selective coating, etc. given by absorber suppliers are not treated as Boundary conditions.

By solving equations (4), (5) and (6) together with boundary conditions simultaneously convection heat transfer rate between outer surfaces of glass envelop and ambient air $\dot{q}_{56conv}$, radiation heat transfer rate between outer surfaces of glass envelop and sky $\dot{q}_{57rad}$ can worked

out.

Equation (7) shows that heat loss of parabolic trough receiver is made up of two parts, namely convection heat transfer rate between the outer surfaces of glass envelop and ambient air $\dot{q}_{56conv}$ and radiation heat transfer rate between outer surfaces of glass envelop and sky $\dot{q}_{57rad}$.

Conduction heat transfers along steel absorber radius $\dot{q}_{23cond}$ and along glass envelop radius $\dot{q}_{45cond}$ are from the Fourier Law, indicated as follows,

$$\dot{q}_{23cond} = \frac{2\pi k_{23}(T_2 - T_3)}{\ln(D_3 / D_2)}$$

$$\dot{q}_{45cond} = \frac{2\pi k_{45}(T_4 - T_5)}{\ln(D_5 / D_4)}$$

Radiation heat transfer in annular space is as follows,

$$\dot{q}_{34rad} = \frac{\sigma\pi D_3(T_3^4 - T_4^4)}{\left(\frac{1}{\varepsilon_3} + \frac{(1-\varepsilon_4)D_3}{\varepsilon_4 D_4}\right)}$$

Convection heat transfer in annular space is as follows [12]:

$$\dot{q}_{34conv} = \pi D_3 h_{34}(T_3 - T_4)$$

While annular pressure $P_{Annular} <\sim 133.28\,Pa$ convection heat transfer is mostly the conduction heat transfer between gas molecules and then heat transfer coefficient $h_{34}$ can be write as follows[10],

$$h_{34} = \frac{k_{std}}{\frac{D_3}{2}\ln\left(\frac{D_4}{D_3}\right) + b\lambda\left(1 + \frac{D_3}{D_4}\right)}$$

While annular pressure $P_{Annular} >\sim 133.28\,Pa$ convection heat transfer inside

annular space is mostly natural convection Raithby-Holland correlations of horizontally natural convection in annular space can be used as convection heat transfer $\dot{q}_{34conv}$ [11],

$$\dot{q}_{34conv} = \frac{2.425k_{34}(T_3 - T_4)\left(\frac{\Pr Ra_{D_3}}{0.861+\Pr_{34}}\right)^{\frac{1}{4}}}{\left(1+\left(\frac{D_3}{D_4}\right)^{\frac{3}{5}}\right)^{\frac{5}{4}}}$$

$$Ra_{D_3} = \frac{g\beta(T_3 - T_4)D_3^{\ 3}}{\alpha\nu}$$

Convection heat transfer between outer surface and ambient $\dot{q}_{56conv}$ is expressed as

$$\dot{q}_{56conv} = h_{56}\pi D_5(T_5 - T_6)$$

$$h_{56} = \frac{k_{56}}{D_5}Nu_{D_5}$$

While wind velocity $v_6 \le 0.1m/s$ 时, wind flow around HCE can be considered as natural convection. Nusselt number $Nu_5$, via Churchill-Chu correlations, can be expressed as [12],

$$\overline{Nu}_{D_5} = \left\{0.60 + \frac{0.387Ra_{D_5}^{1/6}}{\left[1+\left(\frac{0.559}{\Pr_{56}}\right)^{9/16}\right]^{8/27}}\right\}^2$$

While wind velocity $v_6 > 0.1m/s$ 时, wind flow around HCE can be considered as forced convection. Nusselt number $Nu_5$, via Zhukauskas

correlations, can be expressed as [12],

$$\overline{Nu}_{D_5} = C\,\mathrm{Re}_{D_5}^{m}\,\mathrm{Pr}_6^{n}\left(\frac{\mathrm{Pr}_6}{\mathrm{Pr}_5}\right)^{1/4}$$

Radiation heat transfer between outer surface and sky is as follows,

$$\dot{q}_{57rad} = \sigma\pi D_5\varepsilon_5\left(T_5^4 - T_7^4\right)$$

## 5.4. Verification of the model

Off-work method with steady state equilibrium has been used to conduct the experiment in literature 2. The experiment uses two 2 m-length heater assemblies with one cartridge heater and two coil heaters in each heater assembly , and each heater assembly is inserted into the absorber concentrically as a heat source to heat the receiver uniformly and keep the receiver under a thermally steady state[12]. One coil heater is inserted inside receiver and the other coil heater is just outside the end of the receiver. Then equation (3) can be employed to calculate the heat loss to ambient. Parameters of HCE used in literature 2 are shown in tab.6 and used as the parameters of verification of the model. Experimental data used for comparison with the model results are still cited from literature 2, as shown in tab.7

**Tab. 6 parameters of HCE used in this paper**

| characters | UVAC2008 | UVAC3 |
|---|---|---|
| length（m） | 4.06 | |
| Working temperature | Up to 400℃ | |
| coatings | α>0.96, ε<0.1 at 400℃ Cermet (0.10 @ 400C)' | Cermet (0.14 @ 400C)' |
| absorber Inner diameter(m) | 0.066 | |
| absorber outer diameter (m) | 0.07 | |
| Inner diameter of glass envelop (m) | 0.109 | |
| outer diameter of glass envelop (m) | 0.15 | |
| Annular pressure(Pa) | 0.013 | |
| End structure | Bellow lies outside glass envelop | |

Tab.7 Experimental data [2]

| UVAC3 NO.1 | | | | UVAC3 NO.2 | | | |
|---|---|---|---|---|---|---|---|
| ΔT(K) | $T_6$ (K) | Uncert. in ΔT (±K) | Uncert. in Heat Loss (W/m) | ΔT(K) | $T_6$ (K) | Uncert. in ΔT (±K) | Uncert. in Heat Loss (W/m) |
| 133.3 | 22.9 | 1.6 | 8.9 | 126.8 | 23.7 | 1.6 | 8.9 |
| 223.9 | 23 | 1.6 | 8.9 | 171.2 | 23.8 | 1.6 | 8.9 |
| 286.3 | 23.1 | 1.7 | 9.0 | 226.5 | 22.7 | 1.6 | 9.0 |
| 328.5 | 22.7 | 1.8 | 9.1 | 276.9 | 22.9 | 1.6 | 9.1 |
| 377.1 | 23.1 | 1.9 | 9.2 | 276.9 | 23.5 | 1.6 | 9.1 |
| 178.3 | 22.9 | 1.6 | 8.9 | 325.3 | 24 | 1.8 | 9.2 |
| 425.6 | 24.6 | 2.1 | 9.4 | 376.7 | 23.5 | 1.9 | 9.3 |
| | | | | 425.5 | 24.2 | 2.1 | 9.4 |

Fig.23 shows the comparison of experiment data from literature [2] and simulation results of UVAC3. From fig.24 we can see that there are a very small difference between the simulation results and experimental data. The maximum error between simulation results and experiment data is less than 7% and is reasonable. During relatively low temperature difference ΔT, which is the inner surface temperature of absorber $T_2$ minus ambient temperature $T_6$, simulation results is relatively low

because of the heat loss by bellows. During relatively high temperature difference ΔT simulation results is relatively high This is maybe because the emissivity curve of the solar selective absorber is an experimental data curve fit and there is some difference between the emissivity curve and the experimental data, which causes some heat loss difference between the simulation results and experimental data. Additionally, the assumptions for simplifying the mathematic model can also cause some heat loss difference between the simulation results and experimental data. In general simulation results can fit the experimental data very well. Taking the uncertainty of the test, as shown in tab.6, into account the model made in this paper can indicate thermal performance of heat loss and it is feasible for the model to evaluate the thermal performance of heat loss of HCE.

## 5.5 Investigation on UVAC3 and UVAC2008 evacuated receiver and discussions

Tab.6 shows the basic parameters of UVAC3 and UVAC2008. From tab.6 we know that the parameters are almost the same except for the great improvement in coating of UVAC2008. No performance data of UVAC2008 receiver have been found in public documents by now so evaluation of thermal performance of heat loss of UVAC3 and UVAC2008 was conducted and analyzed with parameters in tab.6 in the

following text. Comparisons of results of UAV3 and UVAC2008 are shown in fig.25-34. During the simulation $T_6$=20℃ is assumed.

Fig.24 gives the curves of UVAC3 and UVAC2008 between heat loss and temperature difference ΔT. Curves in fig.24 show that heat loss of UVAC2008 increases still fast with the increase of temperature difference ΔT, but total heat loss of UVAC2008 reduces in large amount in comparison to that of UVAC3 at the same temperature difference ΔT due to the improved selective coating, which means the thermal performance of UVAC2008 increase greatly in contrast with UVAC3. Selective coating performance of UVAC2008 has confirmed this result [13]. So a conclusion can be made that the performance of selective coating of HCE has a great influence on the performance of HCEs. Based on the simulation results a correlation has been developed to predict the heat loss as a function of temperature difference ΔT for UVAC2008 as follows:

$$\dot{q}_{heatloss} = 5\times10^{-9}\Delta T^4 + 10^{-6}\Delta T^3 + 5\times10^{-4}\Delta T^2 + 0.0266\Delta T$$

The correlation is accurate under $\Delta T < 450°C$ and $T_{ambient} < 450°C$.

High-temperature oxidation and other factors during work of HCE will degrade the performance of selective coatings, which cause the increase of emmisivity and decrease of absorptance of selective coatings. The increase of emmisivity and decrease of absorptance of selective coatings will degrade the efficiency and finally cause the disablement of HCE

Fig.25 &26 give the relationship between ambient wind velocity and the total heat loss of UVAC3 and UVAC2008 respectively. Those curves are identical. Fig.26 &27 show that the total heat loss is becoming larger with the increase of wind velocity, but the gradient of the curves is so small that the change of heat loss can not be found while the temperature difference ΔT is low. Change of total heat loss at temperature difference ΔT=377.1K is less than 20W/m with wind velocity increasing from 0m/s to 4.5m/s although the gradient of the heat loss curve is becoming clearer with the temperature difference ΔT becoming larger. This is because with the increase of wind velocity the outer surface temperature of glass envelop reduces in small amount, and then increase of radiation heat transfer through annular space is very small with radiation as dominant heat transfer inside annular space. So the conclusion can be attained that influence of wind velocity on total heat loss of HCE is so small.

With the increase of wind velocity from 0 m/s to 4.5m/s heat transfer form changes from natural convection to turbulent heat transfer, and so there should be a groove during low wind velocity, as shown in fig.27. The groove in fig.27 is right that is because the temperature interval is relatively large in dealing with the transition from natural convection to turbulent convection in literature 12. From the curve in fig.27 we know that when wind velocity increases to some extent convection heat transfer rate will be lower than that in natural convection region, which is

consistent with actual condition.

Fig.28&29 show the relationships between the annular pressure and total heat loss of receiver, from which we know when the annular pressure is above 0.1Pa, especially above 100Pa the total heat loss increases rapidly and trend of curves is identical. The higher the annular pressure is the larger heat loss is.

Fig.30 shows the changes of convection heat transfer, radiation heat transfer and total heat loss through annular space for UVAC2008 with $\Delta T$ equal to 380K. Gas density increases and heat transfer form changes from initially dominant conduction heat transfer between molecules to natural flow, laminar flow and finally to turbulent convection heat transfer when annular pressure increases to 100Pa. when annular pressure is higher than 13328Pa heat transfer rate increases greatly, while radiation heat transfer reduces slowly.

Radiation heat transfer reduces in small amount that is because convection heat transfer increases greatly with the increase of annular pressure, which causes the increase of outer surface temperature of glass envelop. During the increase of annular pressure radiation heat transfer reduces from initial 234.4w/s to 153.3w/m, and its fraction reduces from initial 99.3% to 9%. On the contrary convection heat transfer reduces from initial 1.63w/s to 1544w/m, and its fraction reduces from initial 0.7% to 91% during the increase of annular pressure. Influence of annular

pressure on the radiation heat transfer through annular space can be ignored in contrast with convection heat transfer.

Gas entering annular space through sealing, absorber wall and other possible places can causes the increase of annular pressure and then accelerates degradation of selective coatings and HCE.

Fig.31 shows the comparison of total heat transfer of UVAC3 and UVAC2008 at different wind velocity. We can see that heat loss of UVAC2008 is 66 W/m lower than that of UVAC3 at the same annular pressure, wind velocity and identical temperature difference ΔT, which means thermal performance of UVAC2008, has been improved greatly and wind velocity has a little influence on heat loss of HCE too. Results in fig.31 are consistent with that in fig.26&27.

Fig.32 shows heat loss change of UVAC3 and UVAC208 with annular pressure at identical temperature difference ΔT. As fig.32 shows, annular

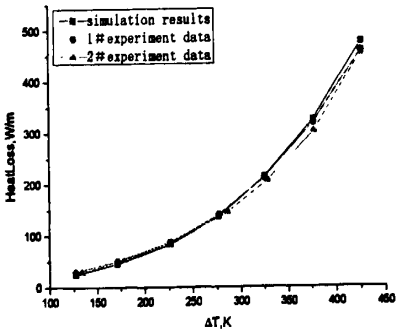


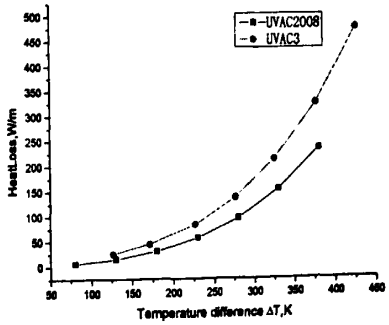

Fig.23 comparison of experiment data and computation results of UVAC3

Fig.24 Heat Loss comparison between UVAC2008 and UVAC3

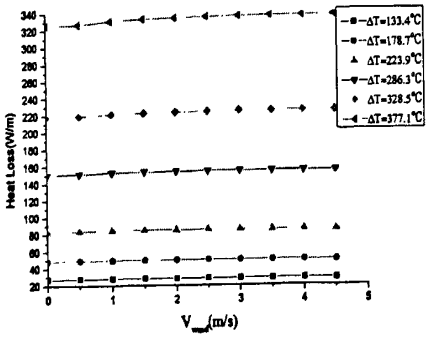


Fig.25 heat loss changes of UVAC3 with wind velocity in different ΔT

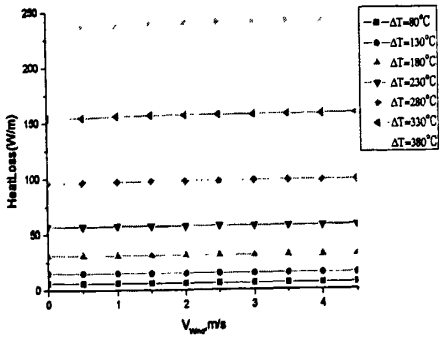


Fig.26 heat loss changes of UVAC2008 with wind velocity in different ΔT

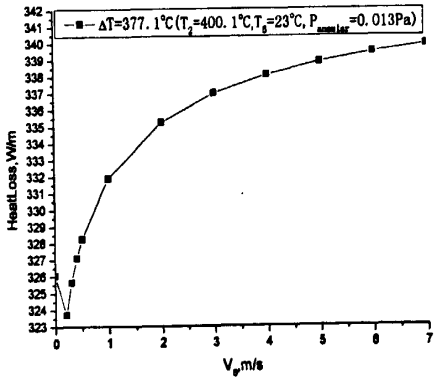


Fig.27 heat loss of UVAC3 changes with wind velocity at $\Delta T=377.1\&P_{annular}=0.013Pa$

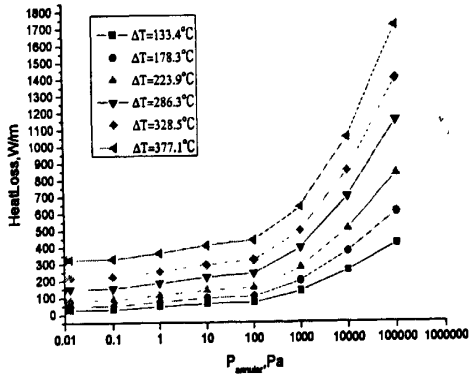


Fig.28 heat loss changes of UVAC3 with $P_{annular}$ in different ΔT

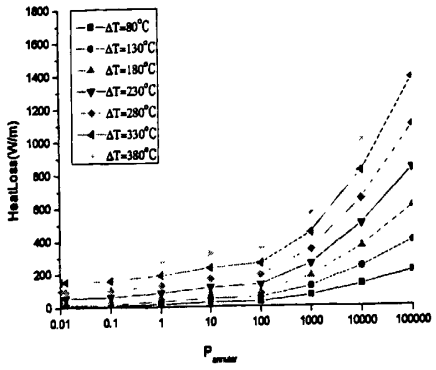


Fig.29 Heat Loss of UVAC2008 changes with annular pressure in different ΔT

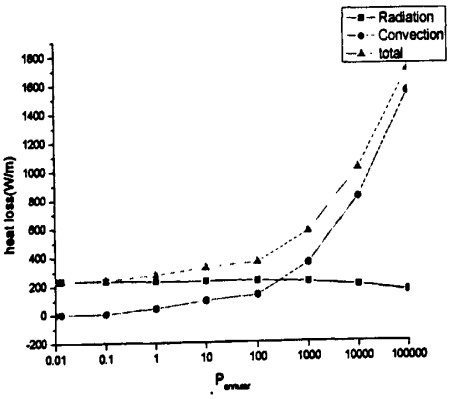


Fig.30 changes of radiation, convection and heat loss of UVAC2008 through annular space with the change of $P_{annular}$

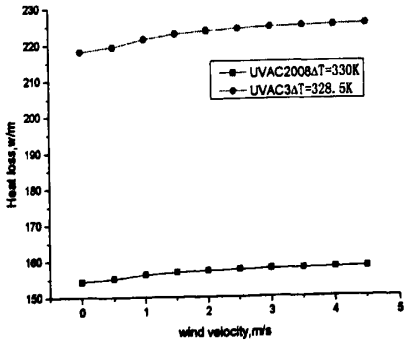


Fig.31 Heat loss comparison of UVAC3 and UVAC2008 in different wind velocity at nearly the same $\Delta T$

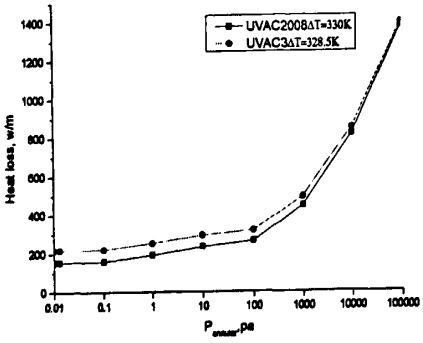


Fig.32 Heat loss comparison of UVAC3 and UVAC 2008 in different $P_{annular}$ at nearly the same$\Delta T$

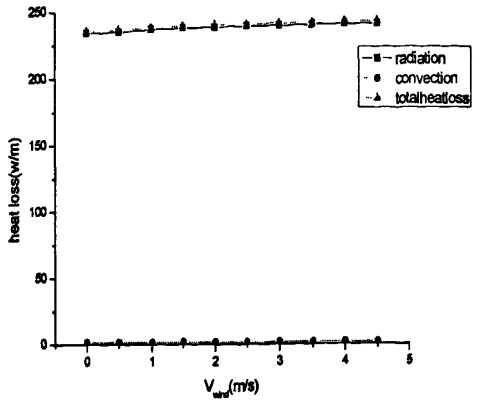


Fig.33 different Heat Loss in annular space at ΔT equal to 380K for a new UVAC2008

Pressure has a great influence on heat loss, and heat loss will be equal to each other when annular space rises to ambient pressure. Fig.33 shows the detailed heat transfer including convection heat transfer, radiation heat transfer and the total heat loss through the annular space at the temperature difference ΔT equal to 380K for a new UVAC2008. Convection heat transfer is very small in contrast to radiation heat transfer with inner surface temperature of absorber at 400℃ for a new UVAC2008.

# Chapter 6 Conclusions

- A two-dimensional empirical model is modeled based on the computation methods and the analysis of heat transfer process of HCE, and simulation results show that the 2D model is accurate and can be used to evaluate the thermal performance of heat loss.
- Thermal performance of heat loss of UVAC3 and UVAC2008 receivers have been evaluated, and simulation results show that performance of selective coatings is one of the most important factors, which has a great influence on thermal performance of heat loss of HCE, and so improvement of selective coating property such as increase of absorbance and decrease of emmitance of selective coatings is one vital way to improve the thermal performance of CHE.
- Annular pressure is another vital factor, which has a great influence total heat loss of receiver too. The higher the annular pressure is the larger heat loss is. Gas density increases and heat transfer form changes from initially dominant conduction heat transfer between molecules to natural flow, laminar flow and finally to turbulent convection heat transfer when annular pressure increases from 0.013Pa to 13328Pa. when annular pressure is higher than 100Pa heat

transfer rate increases greatly. When annular pressure is under 0.013Pa heat transfer by air in annular space is only conduction and can be ignored.

- During the increase of annular pressure radiation heat transfer reduces from initial 234.4w/s to 153.3w/m, and its fraction reduces from initial 99.3% to 9%. On the contrary convection heat transfer reduces from initial 1.63w/s to 1544w/m, and its fraction reduces from initial 0.7% to 91% during the increase of annular pressure. Influence of annular pressure on the heat transfer through annular space can be ignored in contrast with convection heat transfer. So it is very important to prevent gas from entering inside annular space and improve the capacity of getter inside annular space, which can keep the quality of selective coatings as much as possible.
- Influence of wind velocity on thermal performance of heat loss of HCE is very low in contrast with selective coatings and annular space.
- Simulation results show that thermal performance of UVAC2008 is much higher than that of UVAC3.

# Perspectives and Future Job

Besides heat loss testing on the receiver and optical efficiency analysis, several parameters on which the efficiency depends should be studied in details section by section as follow.

According to available surface, wind load test results, mechanical and technical properties of the materials, optimum method for the collector mounting have been selected to:

- Size the geometry of the still structure
- measure the wind speed $V_{wind}$
- determine wind direction α
- determine the law of the influence of the wind angle of attack on the efficiency of the whole collector system.

**Measurement of the Heat Transfer Fluid properties**

- To measure the volume flow rate of the Heat Transfer Fluid $\dot{V}_{oil}$ thus deduct its masse flow rate $\dot{m}_{oil}$, and volume velocity.
- To measure the inlet $T_{in}$ and outlet $T_{out}$ temperatures of the HTF for the receiver tube.
- To calculate collector efficiency.

**Measurement of direct solar radiation** $I_0$

- To measure solar altitude angle, thus determine collecting irradiance $I_s$.

$$I_s = I_0 S \cos\beta$$

- To measure the amount of radiation ( $Q_{in\text{-}abs}$ ) on the surface of receiver tube, thus determine output scatterings radiant energy ($Q_{out\text{-}abs}$) on the surface of receiver tube.

**Measurement techniques for the characterization of the focal region of trough collectors**

The focal region of parabolic trough collectors is extended over the whole length of the concentrator. This complicates the measurement of the flux distribution on the absorber of such solar collectors. However, in order to optimize the solar field output it is essential to study the effects of concentrator precision on the optical performance of the collectors. The intercept factor of radiation with the absorber tubes is a significant measure for this. Research existing techniques found that one the best way consist of using Ray – tracing based on information obtained from photogrammetry.

# References


1 Burkholder, F., Price, H., Brandemuehl, M., Netter, J., Kutscher, C., Wolfrum, E. Parabolic Trough Receiver Thermal Testing. in: Proceedings of ES2007, Energy sustainability 2007. Long Beach, CA, 2007

2 F.Burkholder and C. Kutscher. Heat-Loss Testing of Solel's UVAC3 Parabolic Trough Receiver. In: NREL/TP-550-42394, 2008

3 Dudley, V., Kolb, G., Mahoney, A.R., etc. Test Results SEGS LS-2 Solar Collector. In: SAND94-1884, 1994

4 Moss, T., Brousseau, D. Test Results of a Schott Trough Receiver using a LS-2 Collector. in: Proceedings of ISEC: ASME 2005. Orlando, Florida, 2005

5 H. Price, R. Forristall, T. Wendelin, A. Lewandowski, etc Field Survey of Parabolic Trough Receiver Thermal Performance. In: NREL/CP-550-39459 ,2006

6 Markus Pfänder, Eckhard Lü pfert, Paul Pistor. Infrared temperature Measurements on Solar Trough Absorber Tubes. Solar Energy, 2007. 81:629–635

7 Pfänder, M., Lüpfert, E., Heller, P. Pyrometric Temperature

Measurement on Solar Thermal Receivers. ASME J. Sol. Energy Eng., 2006, 128:285–292

8 Soteris Kalogirou, Stephen Lloyd, John Ward. Modeling, optimisation and performance evaluation of a parabolic trough solar collector steam generation system, Solar Energy, 1997.60(1): 49-59

9 Duffie, J. A.; Beckman, W. A. Solar Engineering of Thermal Processes, Second Edition. New York: John Wiley and Sons. 1991

10 Marshal N., Transl. Gas Encyclopedia. New York: Elsevier,1976

11 Bejan, A. Convection Heat Transfer, Second Edition. New York: John Wiley & Sons,1995

12 Incropera, F.; DeWitt, D. Fundamentals of Heat and Mass Transfer, Third Edition. New York: John Wiley and Sons.2007

13 www.solel.com

14 Allan Lewandowski, Calvin Feik, Ray Hansan, Steve P. Trough Receiver Heat Loss Testing. Presented at the 2006 Parabolic Trough Technology Workshop held on February 14-16 in incline village, Nevada.

15 Cohen G. "Operation and efficiency of large-scale solar thermal power plants", Optical Materials Technology for Energy Efficiency and Solar Energy Conversion, SPIE V2017, 332-337, 1993.

16 Cohen, G. and Kearney, D., " Improved Parabolic Trough Solar

Electric System Based on the SEGS Experience", Proceeding of the 1994 annual conference, ASEC 94, 147-150.

17 Eric C. Guyer, " Handbook of Applied Thermal Design", McGraw-Hill, 1989.

18 Heinzel V., Kungle H. and Simon M. "Simulation of a Parabolic Trough Collector", ISES Solar World Congress,, Harare, Zimbabwe, 1-10, 1995.

19 Lippke, F., "Direct Steam Generation in the Parabolic Trough Solar Power Plants: Numerical Investigation of the Transients and the Control of a Once – Through System", J. of Solar Energy Eng., V118, 9-14, Feb. 1996.

20 Morrison, G. L. and Litvak, A., "Condensed Solar Radiation Data Base For Australia", University of NSW, School of Mechanical and Manufacturing Engineering, Report 1988/FMT/1, Sydney, 1988.

21 F. Burkholder and C. Kutscher . Heat-Loss Testing of Solel's UVAC3 Parabolic Trough Receiver. Technical Report NREL/TP-550-42394 January 2008.

22 Integrated Solar Combined Cycle Systems (ISCCS) Using Parabolic Trough Technology, Phase 1B Technical and Financial Review, Spencer Management Associates, Diablo, CA: March 1996, draft.

23 LUZ. Solar Electric Generating System IX Technical Description, LUZ International Limited: 1990.

24 Lotker, M., Barriers to Commercialization of Large-Scale Solar Electricity: Lessons Learned from the LUZ Experience, Sandia National Laboratories, Albuquerque, New Mexico: 1991. Report SAND91-7014.

25 Winter, C.-J., R. Sizmann, and L. Vant-Hull, eds., Solar Power Plants - Fundamentals, Technology, Systems, Economics. Springer-Verlag, Berlin, 1990, ISBN 3-540-18897-5.

26 O&M Cost Reduction in Solar Thermal Electric Power Plants - Interim Report on Project Status, KJC Operating Company, for Sandia National Laboratories: September 1, 1994.

27 O&M Cost Reduction in Solar Thermal Electric Power Plants - 2nd Interim Report on Project Status, KJC Operating Company, for Sandia National Laboratories: July 1, 1996.

28 Dudley, V., G. Kolb, A. R. Mahoney, T. Mancini, C. Matthews, M. Sloan, and D. Kearney, Test Results: SEGS LS-2 Solar Collector, Sandia National Laboratories, Albuquerque, New Mexico: December 1994. Report SAND94-1884.

29 Cohen, G., and S. Frier, "Ten Years of Solar Power Plant Operation in the Mojave Desert", Proceedings of Solar 97, the 1997 ASES Annual Conference, Washington, D.C. (April, 1997).

30 Fugitive Emissions Testing - Final Report, AeroVironment, Inc., for KJC Operating Company, Monrovia, CA: January 1995.

31 Texas Renewable Energy Resource Assessment: Survey, Overview & Recommendations, Virtus Energy Research Associates, for the Texas Sustainable Energy Development Council, July, 1995, ISBN 0-9645526-0-4.

32 Williams, T., M. Bohn, and H. Price, "Solar Thermal Electric Hybridization Issues", Proceedings of the ASME/JSME/JSES International Solar Energy Conference, Maui, HI (March 19-24, 1995).

33 Muller, M., Direct Solar Steam in Parabolic Trough Collectors (DISS), Plataforma Solar de Almeria (PSA), CIEMAT and DLR, May, 1994, ISBN 84-605-1479-X.

34 Marion, W., and S. Wilcox, Solar Radiation Data Manual for Flat-Plate and Concentrating Collectors, National Renewable Energy Laboratory, Golden, Colorado: April 1994. Report NREL/TP-463-5607.

35 Kearney, D., and C. Miller, Solar Electric Generating System VI - Technical Evaluation of Project Feasibility, LUZ Partnership Management, Inc.: January 15, 1988.

36 A.Valdes,Metropolitan Autonomous University, private communication, 2000

37 Martinez, Parabolic trough concentrator with first surface mirrors for power plant of the Engineering Institute UNAM, Master's degree Thesis, Mexico, 1999

38 T. Fend, K.Wenzel, (1999). Optical Measurements in the focal area of a parabolic trough concentrator, J Phys. IV (France) (1999) 605

39 Euro Trough project. Final Public Report, European Commission Contract No. JOR3-CT98-00231, Servilla / Almeria /Brussels, 2001

40 Yaghoubi M, Azizian K, Rahi M. Use of Shiraz power plant for various alternative applications. In: Proceedings of the first international exergy, energy and environment symposium. Izmir, Turkey, 2003. p. 128.

41 Kearney D. Status of the SEGS plants. Los Angeles, CA, USA: Luz International Limited; 1992.

42 Yaghoubi M, Velayati E. Undeveloped convective heat transfer from an array of cubes in cross-stream direction. Int J Therm. Sci. 2005;44:756–65.

43 Naeeni N, Yaghoubi M. Analysis of wind flow around a parabolic collector

44 Fluid flow. Renewable Energy An Int J, submitted for publication.

45 Bejan A. Convection heat transfer. New York: Wiley; 2004. p. 178–83.

46 G. Cohen, Achievements in Solar Parabolic Trough Technology

Proceedings of the 7th International Symposium on Solar Thermal Concentrating Technologies, Moscow, Russia, September 1994.

47 G. Cohen and D. Kearney, Improved Parabolic Trough Solar Electric Systems Based on the SEGS Experience, Proceedings of the 1994 Annual Conference of the American Solar Energy Society (Solar 94), San Jose, California, June 1994.

48 R. J. Nelson and R. G. Cable, The KJC Plant Performance Model – An Improved SEGS Plant Simulation, Proceedings of the ASME/JSME/JSES/KSME International Conference, Maui, Hawaii, April 11–14, 1999.

49 Riffelmann, K.-J., Ulmer, S., and Neumann, A., 2004, "Performance Enhancement of Parabolic Trough Collectors by Solar Flux Measurement in the Focal Region," Proceedings of the 12th SolarPACES International Symposium, Oaxaca, Mexico, October 6–8.

50 Rabl, A., 1985, Active Solar Collectors and Their Applications. Oxford University Press, New York.

51 J. W. Twidell and A.D. Weir, Renewable Energy Resources, London 86

52 M. M. Mukhitdinov and S.F. Ergashev, Solar Parabolic Trough Plants (in Russia), Tashkent: Fan; 1995.

# Nomenclature

HCE – Heat Collecting Element

HTF – Heat Transfer Fluid

TC - Temperature Controller

TRSF – Transformer

DAS – Data acquisition System

$\dot{q}_{col}$ Total collector thermal energy output, W/m

$\dot{q}_{abs}$ Absorbed thermal energy of HCE, $W/m^2$

$h_{in}$ Enthalpy of heat transfer fluid in inlet of HCE,

$h_{out}$ Enthalpy of heat transfer fluid in outlet of HCE,

$q_m$ Mass flow rate of heat transfer fluid,$m^3/s$

$P_{heatsource}$ Power of heat source, W;

$P_{heaters,input}$ Power of heaters, W;

$\dot{q}_{56conv}$ Convection heat transfer rate between outer surface of glass envelop and ambient air per meter receiver length, W/m;

$\dot{q}_{57rad}$ radiation heat transfer rate between outer surface of glass envelop and sky per meter receiver length, W/m;

$\dot{q}_{45cond}$ conduction heat transfer rate through glass envelop wall per meter receiver length, W/m;

$\dot{q}_{34conv}$ Convection heat transfer rate between outer surface of steel

absorber and inner surface of glass envelop per meter receiver length, W/m;

$\dot{q}_{34rad}$ radiation heat transfer rate between outer surface of steel absorber and inner surface of glass envelop per meter receiver length, W/m;

$\dot{q}_{23cond}$ conduction heat transfer rate through steel absorber wall per meter receiver length, W/m;

$\dot{q}_{HeatLoss}$ total heat transfer rate between outer surface of glass envelop and ambient per meter receiver length, W/m;

$h_{34}$ Convection heat transfer coefficient of annulus gas at T34 in annular space, W/m2-K;

$h_{56}$ Convection heat transfer coefficient of air at T56 around the horizontal glass envelop, W/m2-K

$D_2$ inside diameter of absorber pipe, m;

$D_3$ outside diameter of absorber pipe, m;

$D_4$ inside diameter of glass envelop, m;

$D_5$ outside diameter of glass envelop, m;

$T_2$ absorber pipe inner surface temperature, K;

$T_3$ absorber pipe outer surface temperature, K;

$T_4$ glass envelope inner surface temperature, K;

$T_5$ glass envelope outer surface temperature, K;

$T_6$ ambient temperature, K;

$T_7$ estimated effective sky temperature, K;

$T_{34}$ Average temperature of annulus gas, $T_{34}=\frac{T_3+T_4}{2}$, K;

$\Delta T$ inner surface temperature $T_2$ minus ambient temperature $T_6$, K;

$T_{56}$ average temperature of air, $T_{56}=\frac{T_5+T_6}{2}$, K;

$Nu_{D_2}$ Nusselt number of HTF based on D2;

$Nu_{D_5}$ Nusselt number of air based on D5;

$\varepsilon_3$ emissivity of absorber selective coating;

$\varepsilon_4$ emissivity of inner surface of glass envelope;

$\varepsilon_5$ emissivity of outer surface of glass envelope;

$k_{23}$ thermal conductance of absorber wall at $T_{23}=\frac{(T_2+T_3)}{2}$, W/m-K;

$k_{34}$ Thermal conductance of annulus gas at $T_{34}=\frac{(T_3+T_4)}{2}$, W/m-K;

$k_{45}$ Thermal conductance of glass at $T_{45}=\frac{(T_4+T_5)}{2}$, W/m-K;

$k_{std}$ thermal conductance of annulus gas at standard temperature and pressure, W/m-K;

$k_{56}$ thermal conductance of air at $T_{56}=\frac{(T_5+T_6)}{2}$, W/m-K;

$Pr_2$ Prandtl number of HTF evaluated at T2;

$Pr_{34}$ Prandtl number of annulus gas at T34;

Pr5 Prandtl number of air at T5

$Pr_{56}$ Prandtl number for air at T56;

Pr6 Prandtl number of air at T6

$Ra_{D_3}$ Rayleigh number of annulus gas based on D3;

$Ra_{D_5}$ Rayleigh number of air based on D5;

$P_{Annular}$ Annular gas pressure, Pa;

$\sigma$ Stefan-Boltzmann constant, $\sigma = 5.67 \times 10^{-8}$, $W/m^2\text{-}K^4$;

# Published Papers

1 TRAORE, M. K., 熊亚选，吴玉庭，马重芳. 槽式太阳能集热管热性能评估方法. 太阳能 2009 年 5 月

2 熊亚选, MODIBO K. T., 吴玉庭, 马重芳. 槽式太阳能聚光集热技术 太阳能 2009 年 6 月

3 熊亚选，吴玉庭, 马重芳, MODIBO K. T. 槽式太阳能集热管传热损失性能的数值研究，中国科学 E 辑：技术科学，2009（已录用，EI 收录期刊）

4 熊亚选，吴玉庭，马重芳，TRAORE, M. K., Numerical Investigation of Thermal Performance of Heat Loss of Parabolic Trough Receiver，Science in China Series E: Technological Sciences，2009（accepted, SCI Source Journal）

# Acknowledgments

Foremost, I would like to express my sincere gratitude to my advisor Prof. CHONG FANG MA for the continuous support of my PhD study and research, for his patience, motivation, enthusiasm, and immense knowledge. His guidance helped me in all the time of research and writing of this thesis. I could not have imagined having a better advisor and mentor for my PhD study.

Besides my advisor, I would like to thank Prof. Wu Yu Ting for his encouragement, insightful comments, and hard questions.

I thank my fellow lab mates: Dr Xiong Yaxuan, Dr Xu Lixian, and Dr Liu Bin for the stimulating discussions, for the sleepless nights we were working together before deadlines, and for all the fun we have had in the last four years. Also I thank my Ms Hao in the international exchange center of Beijing University of Technology.

In particular, I am grateful to Mr Hamadoun Toure, diplomatic adviser in charge of students of Malian Embassy in Beijing, for enlightening me the first glance of research。

Last but not the least; I would like to thank my family: my parents Haman Traore, Youma Traore for giving birth to me at the first place and supporting me spiritually throughout my life.